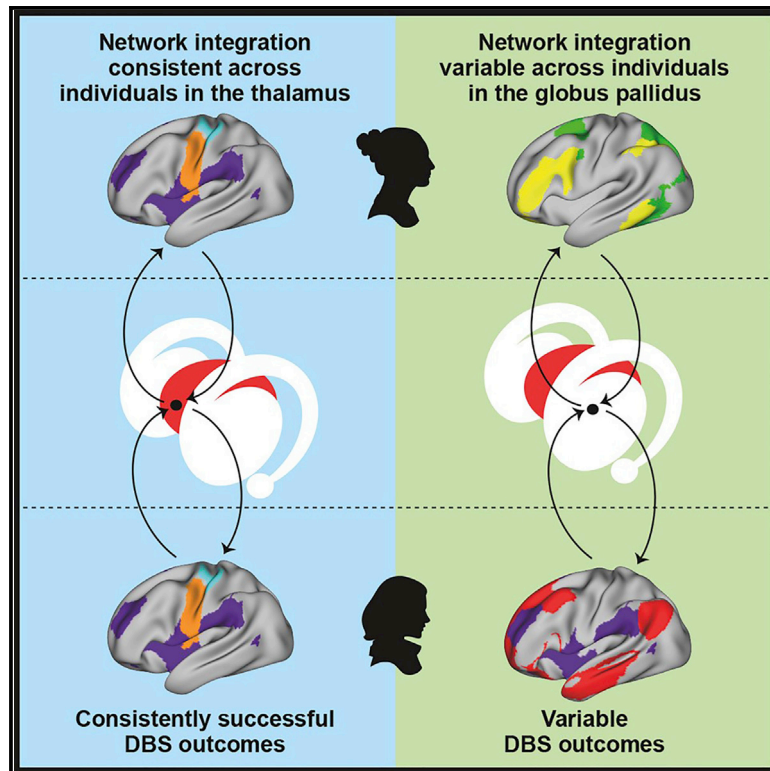# Neuron

Integrative and Network-Specific Connectivity of the Basal Ganglia and Thalamus Defined in Individuals

Graphical Abstract

Authors

Deanna J. Greene, Scott Marek,
Evan M. Gordon, ...,
Bradley L. Schlaggar,
Steven E. Petersen,
Nico U.F. Dosenbach

Correspondence

dgreene@wustl.edu (D.J.G.),
smarek@wustl.edu (S.M.),
dosenbachn@wustl.edu (N.U.F.D.)

In Brief

Individual functional mapping of the human subcortex revealed network integration zones (motor, cognitive, visual attention) that were variable and consistent across people. These individualized maps of cortico-subcortical circuits may have immediate clinical translation for invasive personalized treatments (e.g., deep brain stimulation).

Highlights

- Precision functional mapping identifies subcortical integration zones in individuals

- Systematic connectivity reveals motor, cognitive, and visual attention integration zones

- Subcortical functional organization has individually variable and conserved features

- Integration zones map onto variably effective DBS sites, suggesting clinical utility

CellPress

Neuron

Article

Integrative and Network-Specific Connectivity of the Basal Ganglia and Thalamus Defined in Individuals

Deanna J. Greene,[1,2,20,21,*] Scott Marek,[3,20,*] Evan M. Gordon,[4,5,6] Joshua S. Siegel,[1] Caterina Gratton,[7,8]
Timothy O. Laumann,[1] Adrian W. Gilmore,[12] Jeffrey J. Berg,[9] Annie L. Nguyen,[3] Donna Dierker,[2] Andrew N. Van,[3]
Mario Ortega,[3] Dillan J. Newbold,[3] Jacqueline M. Hampton,[1] Ashley N. Nielsen,[10] Kathleen B. McDermott,[2,11]
Jarod L. Roland,[12] Scott A. Norris,[3] Steven M. Nelson,[4,5,6] Abraham Z. Snyder,[2,3] Bradley L. Schlaggar,[13,14,15]
Steven E. Petersen,[2,3,12,16,17] and Nico U.F. Dosenbach[2,3,17,18,19,*]

[1]Department of Psychiatry, Washington University School of Medicine, St. Louis, MO, USA
[2]Mallinckrodt Institute of Radiology, Washington University School of Medicine, St. Louis, MO, USA
[3]Department of Neurology, Washington University School of Medicine, St. Louis, MO, USA
[4]VISN17 Center of Excellence for Research on Returning War Veterans, Waco, TX, USA
[5]Center for Vital Longevity, School of Behavioral and Brain Sciences, University of Texas at Dallas, Dallas, TX, USA
[6]Department of Psychology and Neuroscience, Baylor University, Waco, TX, USA
[7]Department of Psychology, Northwestern University, Evanston, IL, USA
[8]Department of Neurology, Northwestern University, Evanston, IL, USA
[9]Department of Psychology, New York University, New York, NY, USA
[10]Institute for Innovations in Developmental Sciences, Northwestern University, Chicago, IL, USA
[11]Department of Psychological and Brain Sciences, Washington University, St. Louis, MO, USA
[12]Department of Neurological Surgery, University of California, San Francisco, San Francisco, CA, USA
[13]Kennedy Krieger Institute, Baltimore, MD, USA
[14]Department of Neurology, Johns Hopkins University School of Medicine, Baltimore, MD, USA
[15]Department of Pediatrics, Johns Hopkins University School of Medicine, Baltimore, MD, USA
[16]Department of Neuroscience, Washington University School of Medicine, St. Louis, MO, USA
[17]Department of Biomedical Engineering, Washington University, St. Louis, MO, USA
[18]Department of Pediatrics, Washington University School of Medicine, St. Louis, MO, USA
[19]Program in Occupational Therapy, Washington University, St. Louis, MO, USA
[20]These authors contributed equally
[21]Lead Contact
*Correspondence: dgreene@wustl.edu (D.J.G.), smarek@wustl.edu (S.M.), dosenbachn@wustl.edu (N.U.F.D.)
https://doi.org/10.1016/j.neuron.2019.11.012

SUMMARY

The basal ganglia, thalamus, and cerebral cortex form an interconnected network implicated in many neurological and psychiatric illnesses. A better understanding of cortico-subcortical circuits in individuals will aid in development of personalized treatments. Using precision functional mapping—individual-specific analysis of highly sampled human participants—we investigated individual-specific functional connectivity between subcortical structures and cortical functional networks. This approach revealed distinct subcortical zones of network specificity and multi-network integration. Integration zones were systematic, with convergence of cingulo-opercular control and somatomotor networks in the ventral intermediate thalamus (motor integration zones), dorsal attention and visual networks in the pulvinar, and default mode and multiple control networks in the caudate nucleus. The motor integration zones were present in every individual and correspond to consistently successful sites of deep brain stimulation (DBS; essential tremor). Individually variable subcortical zones correspond to DBS sites with less consistent treatment effects, highlighting the importance of PFM for neurosurgery, neurology, and psychiatry.

INTRODUCTION

The thalamus and basal ganglia interconnect distant parts of the cerebral cortex via cortico-thalamo-cortical and cortico-striato-thalamic loops (Alexander et al., 1986). Hence, even small lesions in the thalamus or basal ganglia can be neurologically devastating, but similarly sized lesions in the cerebral cortex may go unnoticed (Bogousslavsky et al., 1988; Corbetta et al., 2015; Siegel et al., 2014). Because of their centrality, cortico-striato-thalamo-cortical loops also appear to underlie many neurological and psychiatric disorders, including Parkinson disease, Tourette syndrome, and obsessive-compulsive disorder

(Albin et al., 1989; Bradshaw and Sheppard, 2000; Mink, 2001). Thus, a better understanding of the functional organization of the thalamus and basal ganglia and their connectivity to the cortex is essential for understanding typical and atypical brain function.

Much of our current understanding of the anatomical connections and functional organization of the basal ganglia and thalamus originates from lesion, unit recording, and tracer studies in non-human primates (Alexander and Crutcher, 1990; Haber, 2003; Selemon and Goldman-Rakic, 1985). This work originally suggested that parallel and segregated cortico-striato-thalamic circuits support different functional processes (e.g., motor, cognitive, limbic) (Alexander and Crutcher, 1990; Alexander et al., 1986, 1990). This model has since been updated to account for findings demonstrating convergence of multiple spatially distant cortical projections to the subcortex, describing the circuits as "parallel and integrative" rather than purely parallel (Averbeck et al., 2014; Haber, 2003, 2016). Moreover, there is anatomical evidence from non-human primates that both cortical and cerebellar projections are integrated within the basal ganglia (Bostan and Strick, 2018). Thus, subcortical structures have been posited to contain sites/zones of integration of multiple functions, including executive control, reward processing, and spatial attention (Haber, 2016; Jarbo and Verstynen, 2015).

Neuroimaging studies have aimed to characterize human cortico-subcortical systems in light of the results from non-human primate studies. Much of this work has described segregated functional areas within subcortical structures based on functional and structural connectivity with the cerebral cortex, often defining each area by its preferential connectivity with a particular cortical region or network. These findings have been broadly consistent with the animal data, recapitulating sensorimotor, cognitive, and limbic subdivisions (Arsalidou et al., 2013; Barnes et al., 2010; Behrens et al., 2003; Choi et al., 2012; Di Martino et al., 2008; Fair et al., 2010; Greene et al., 2014; Lehéricy et al., 2004; Zhang et al., 2008). Several studies have also supported the idea that subcortical subregions receive converging projections from multiple distinct cortical regions (Choi et al., 2017; Draganski et al., 2008; Hwang et al., 2017; Jarbo and Verstynen, 2015), which is consistent with the integrative model of cortico-subcortical circuitry (Haber, 2003).

The biggest caveat for all of the structural and functional connectivity studies of the basal ganglia and thalamus in humans, including our own, has been their reliance on group-averaged data. This approach was necessary because of the combination of small quantities of data per individual and the low signal-to-noise ratio (SNR) of MRI. Although group-average designs are valuable for understanding broad principles of subcortical functional organization, the specific organization of each individual is necessarily obscured. For example, the appearance of integration zones across functional networks in large samples may have been an artifact of individual variability rather than the true integration of signals from multiple networks. Because the basal ganglia and thalamus are relatively small structures, such features of functional organization specific to individuals are most prone to obfuscation by group averaging.

Individualized measures of integration and segregation of functional networks in the subcortex have the potential for significant clinical utility. For instance, subcortical structures are targeted using deep brain stimulation (DBS) for treatment of several neurological and psychiatric disorders, including essential tremor, Parkinson disease, dystonia, Tourette syndrome, obsessive-compulsive disorder, and treatment-resistant depression (Baizabal-Carvallo et al., 2014; Dandekar et al., 2018; Mink, 2009; Perlmutter and Mink, 2006; Skogseid, 2014; van Westen et al., 2015). However, specific target structures have variable success rates (McIntyre and Hahn, 2010; Wichmann and Delong, 2011). DBS of the ventral intermediate nucleus of the thalamus for treatment of essential tremor results in over 80% tremor reduction in all patients (Ondo et al., 1998; Perlmutter and Mink, 2006), whereas stimulation of the globus pallidus for treatment of dystonia results in only 30%–50% symptom improvement across all patients and more than 75% improvement in only 33% of patients (Starr et al., 2006; Vidailhet et al., 2005). Thus, an individualized approach for characterizing the functional organization of the subcortex should shed new light on these variable response rates and potentially aid rapid clinical translation toward targeted individualized intervention.

A recent series of studies using precision functional mapping (PFM; collecting large quantities of fMRI data in individuals) characterized the functional architecture of the cerebral cortex and cerebellum in individuals (Braga and Buckner, 2017; Filevich et al., 2017; Gordon et al., 2017b, 2018; Gratton et al., 2018; Laumann et al., 2015; Marek et al., 2018; Poldrack et al., 2015). These studies have shown that the topographies of individual functional brain networks are reliable, externally valid, and stable within an individual and demonstrate individual-specific topological features of brain organization not evident in group-averaged data. Indeed, each individual differs systematically from the group average at particular cortical locations (Seitzman et al., 2019). If a similar degree of individual-specific functional network organization is present in the subcortex, accurately characterizing that organization could advance success rates of treatments like DBS.

The goal of the present study was to investigate the functional organization of the individual human basal ganglia and thalamus. Using the highly sampled individuals from the Midnight Scan Club (MSC) dataset (Gordon et al., 2017b), we implemented a network-based functional connectivity approach to examine (1) functional network specificity and integration within the subcortex and (2) individual variability and similarity of functional organization across subjects. This PFM approach aids in the advancement of our understanding of individual cortico-subcortical systems and may be clinically relevant for more precise, patient-specific treatment of neurological and psychiatric disorders.

RESULTS

To measure cortico-subcortical resting-state functional connectivity (RSFC) in ten highly sampled individuals from the MSC dataset, blood oxygen level-dependent (BOLD) activity time courses were extracted from each voxel in the basal
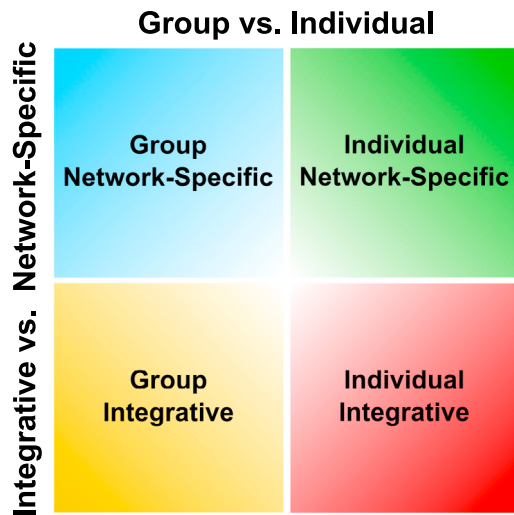
Group vs. Individual

Figure 1. Framework for Subcortical Functional Organization
Subcortical RSFC was characterized along two principal axes, each with two levels (group versus individual, network-specific versus integrative). Group refers to RSFC that is common across participants, whereas individual refers to RSFC that is individual-specific. Network-specific refers to regions of the subcortex with preferential RSFC to a single cortical network, whereas integrative refers to regions of the subcortex with preferential RSFC to multiple cortical networks.

ganglia and thalamus. Cortical time series were averaged across all vertices in each of nine canonical functional networks (Greene et al., 2014; Power et al., 2011), defined for each individual: visual, somatomotor hand, somatomotor face, cingulo-opercular, frontoparietal, dorsal attention, ventral attention, salience, and default mode (STAR Methods; Figure 8). A subcortical voxel-to-cortical network connectivity matrix was generated for each subject by computing the Pearson correlation between the time courses (concatenated across sessions) of each subcortical voxel and each cortical network. These connectivity matrices were used for all subsequent analyses. Given the small size of subcortical structures, additional highly sampled, high-resolution BOLD data (2.6-mm isotropic voxels) were collected from one of the individuals (MSC06) to validate the results.

Our report focuses on two major properties of cortico-subcortical RSFC: (1) network specificity (preferential connectivity with a single network) versus integration (strong connectivity with multiple networks) and (2) group (common organization across individuals) versus individual (variable across individuals) (Figure 1).

RSFC Reliability Requires Larger Amounts of Data in the Subcortex Than in the Cortex
We addressed whether cortico-subcortical RSFC can be measured reliably in individuals using iterative split-half comparisons. Cortico-subcortical correlations were reliable for each individual in each subcortical structure of interest ($r > 0.6$ averaged across all voxels within each structure) with ~100 min of motion-censored data per subject (Figure S1A). More specifically, with more than 100 min of data, 87% of voxels in the caudate, 74% in the putamen, 54% in the globus

pallidus, and 63% in the thalamus had high reliability ($r > 0.70$) (Figure S1B). Low reliability in certain voxels was likely driven by the low temporal SNR (tSNR) in these regions because correlations between reliability and tSNR were significant for all subjects (mean $r = 0.20$, all $p < 0.001$). These results indicate that more data are needed to achieve high reliability for cortico-subcortical RSFC than for cortico-cortical RSFC (45 min, as reported in Gordon et al., 2017b), and cortico-cerebellar RSFC (90 min, as reported in Marek et al., 2018), consistent with Noble et al. (2017).

Subcortical RSFC Is Measurable at the Individual Level
Figure 2A displays group-averaged correlation maps within the subcortex for each cortical network, and Figure 2B displays the correlations from two representative subjects; all subjects are shown in Figure S2. To determine the robustness of the spatial patterns of these correlations, we compared the observed spatial patterns of correlations to those generated from a null distribution from rotated networks on the cortex. Spearman's rho between the actual correlations and percent stronger than null across all networks and subjects was 0.79 ± 0.07 (see STAR Methods for details).

Across subjects, there was similarity in subcortical RSFC for each network (Figure 2C). The default mode network was strongly functionally connected to the medial thalamus and large portions of the caudate extending into the ventral striatum. The visual and dorsal attention networks exhibited strong connectivity with the lateral and posterior regions of the thalamus corresponding to the location of the pulvinar and, possibly, the lateral geniculate nucleus. The frontoparietal and salience networks were functionally connected to the caudate (head, body). The ventral attention network was connected to the caudate, medial putamen, and medial thalamus, with stronger correlations in the left hemisphere. The cingulo-opercular network exhibited strong connectivity with a large portion of the ventral thalamus and distinct anterior and posterior parts of the putamen. Connectivity with the somatomotor networks was observed in the ventral and lateral portions of the thalamus, likely corresponding to ventral lateral and ventral posterior nuclei, with the somatomotor hand network peak correlations shifted posterior to that of the somatomotor face network (consistent with known somatotopy), although there was substantial overlap. In addition to these commonalities, variability across individuals was also evident (Figure S2). For example, Figure 2B shows strong connectivity with the dorsal attention network in the caudate in MSC02 but not in MSC04.

The spatial pattern of correlations was compared with task fMRI responses elicited in the same individuals (Figure 2D; Figure S3). Task activations/deactivations validated the RSFC mapping of functional networks in the subcortex. Deactivations during a set of cognitive/perceptual tasks overlapped well with default mode network connectivity in the head of the caudate and medial thalamus. Activations during these cognitive/perceptual tasks in the subcortex overlapped multiple control networks (e.g., cingulo-opercular, frontoparietal, ventral attention, dorsal attention, salience), sparing the default mode network (Figure S4). In addition, activations in the subcortex in response to hand movements during a motor task (hand > foot
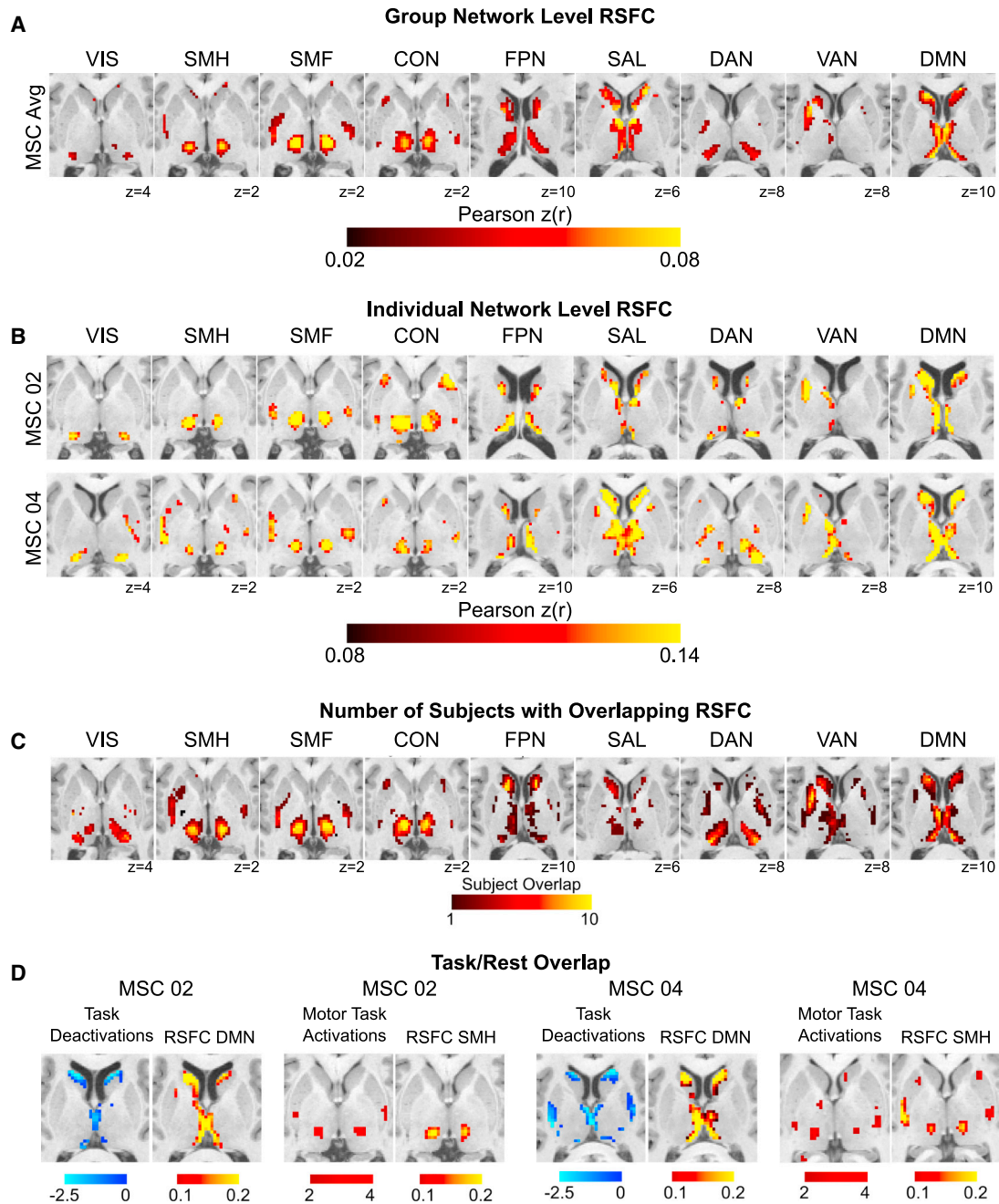
Figure 2. Subcortical RSFC Is Measurable at the Individual Level

(A) Group-averaged subcortical RSFC for each cortical network.

(B) Individual-level subcortical RSFC for each network from two representative MSC subjects, one male (MSC02) and one female (MSC04) (see Figure S2 for all ten subjects).

(C) Subject overlap showing the number of subjects with strong (top 10%) correlations with each network at that voxel.

(D) Concordance between RSFC and task activations/deactivations within individuals. Shown are task-evoked increases in BOLD activity during a motor task converge with peak RSFC in the somatomotor hand network. Task-evoked deactivations during a set of cognitive/perceptual tasks converge with peak RSFC in the default mode network. Anatomical left is image left. VIS, visual; SMH, somatomotor hand; SMF, somatomotor face; CON, cingulo-opercular network; FPN, frontoparietal network; SAL, salience; DAN, dorsal attention network; VAN, ventral attention network; DMN, default mode network.

contrast) overlapped well with positive correlations with the somatomotor hand network.

Individual-Specific and Group-Level Features of Subcortical RSFC

Given that subcortical correlations show individual-specific features (Figures 2B and S2) and consistency across subjects (Figure 2C), we quantified the extent to which functional networks exhibited group versus individual-specific features, using a similarity analysis as in Gratton et al. (2018) and Marek et al. (2018). For each subject, the RSFC data were randomly split in half, and the spatial similarity (Pearson r) of subcortical-cortical correlations with each network was calculated within each subject and between all subjects. To quantify variance in RSFC data shared across individuals (group effect) versus variance unique to individuals (individual effect), we compared the within-individual similarities (on-diagonal elements, individual effect) to the between-individual similarities (off-diagonal elements, group effect), normalized by the sum of the group and individual effects. We conducted this analysis separately for the basal ganglia and thalamus and demonstrated large group contributions (basal ganglia, 42% shared RSFC variance across subjects; thalamus, 39%) and individual contributions (basal ganglia, 58% RSFC variance specific to individuals; thalamus, 61%) (Figure S5). Some control networks (frontoparietal, salience, dorsal attention, ventral attention) showed significantly less similarity across the group (i.e., more individual variability) than the somatomotor networks and the cingulo-opercular network ($\Delta z = -0.43$, $t = -25.15$, p < 0.001). Thus, the cingulo-opercular network stands in contrast to other control networks, demonstrating greater similarity to somatomotor networks in the subcortex.

Localization of Functional Integration Zones in the Subcortex

Previous characterizations of basal ganglia and thalamic functional organization, using group-averaged data, often implemented a winner-take-all network approach (e.g., Choi et al., 2012; Greene et al., 2014; Zhang et al., 2008). This winner-take-all approach cannot account for integration of multiple networks within regions of the subcortex (Haber, 2016) because the functional maps are solely based on the network with the strongest connectivity. In addition, a group-level approach to identifying functional integration could be spuriously affected by averaging across-subject variability. That is, the same anatomical location may exhibit connectivity to different networks in different individuals (Argall et al., 2006; Laumann et al., 2015; Van Essen, 2005), leading to the appearance of integration when those individual signals are averaged together. Therefore, we evaluated network co-localization at the individual level to more accurately characterize the nature of functional integration within the subcortex.

We define integration as exhibiting strong functional connectivity with multiple networks. We implemented a modified winner-take-all analysis approach to account for zones of integration as well as zones that are "network-specific" (one network dominates). For every subcortical voxel, we identified the cortical network with the strongest correlation, as in a stan-

dard winner-take-all procedure. In accordance with Marek et al. (2018), we identified regions of integration versus network specificity by testing whether the RSFC with any other network was above a given threshold (66.7%) of the correlation with the winning network. We tested additional thresholds (50%, 75%), which yielded similar zones of integration (Figure S6A). If the correlations with all the other networks were below this threshold for a given voxel, then that voxel was considered network-specific. If the correlations with any of the other networks were within that threshold for a given voxel, that voxel was considered "integrative" because multiple networks correlated strongly. An alternative approach based on effect size rather than percent differences yielded very similar results (Figure S6B).

Figures 3A and 3B display the subcortical network map for two representative subjects, and Figure 3C shows the group average. All subjects are shown in Figure S7. From the group average maps alone, one might suspect that the zones of integration could be artifactual because of subject averaging. However, we show that several integration zones were identified within all individuals and, thus, are not simply by-products of group averaging. One of the most notable integration zones was identified in the ventral intermediate thalamus, integrating the cingulo-opercular, somatomotor hand, and somatomotor face networks (Figure 3D).

These functional network maps suggest that certain zones of integration and network specificity appear similar across individuals. We quantified the overlap of integrative and network-specific voxels (irrespective of the specific network association) across subjects. Figure 4A displays the overlap of integrative voxels, demonstrating that certain zones were integrative in most subjects (e.g., ventral intermediate thalamus), and Figure 4B shows network-specific voxels, demonstrating that certain zones were network-specific in most subjects (e.g., head of the caudate). In addition, certain integrative or network-specific zones represented the same networks across individuals, whereas others represented different networks across individuals. We further explore this individual similarity and variability in network associations below.

To benchmark the degree of integration in the basal ganglia and thalamus compared to the cerebellum and cerebral cortex, we computed the percent of voxels/vertices within each brain structure that were integrative, as defined by the 66.7% threshold used in the analyses above. This computation demonstrated that a greater percentage of the subcortex (45%) was integrative compared to the cerebellum (35%) and cerebral cortex (31%). Within the subcortex, we found that the thalamus was 45% integrative, the globus pallidus was 52% integrative, the putamen was 42% integrative, and the caudate was 37% integrative. Note that the thalamus was more integrative than the caudate even though the thalamus is 240% larger in size. Therefore, the increased integration in the subcortex is not likely caused by the smaller size of the structures.

To ensure that integration was not driven by methodological factors, we tested different numbers of *a priori* cortical networks (i.e., 7 and 15 networks derived from Infomap) as well as the effect of proximity to multiple networks (i.e., voxels with a greater number of distinct networks surrounding it would be
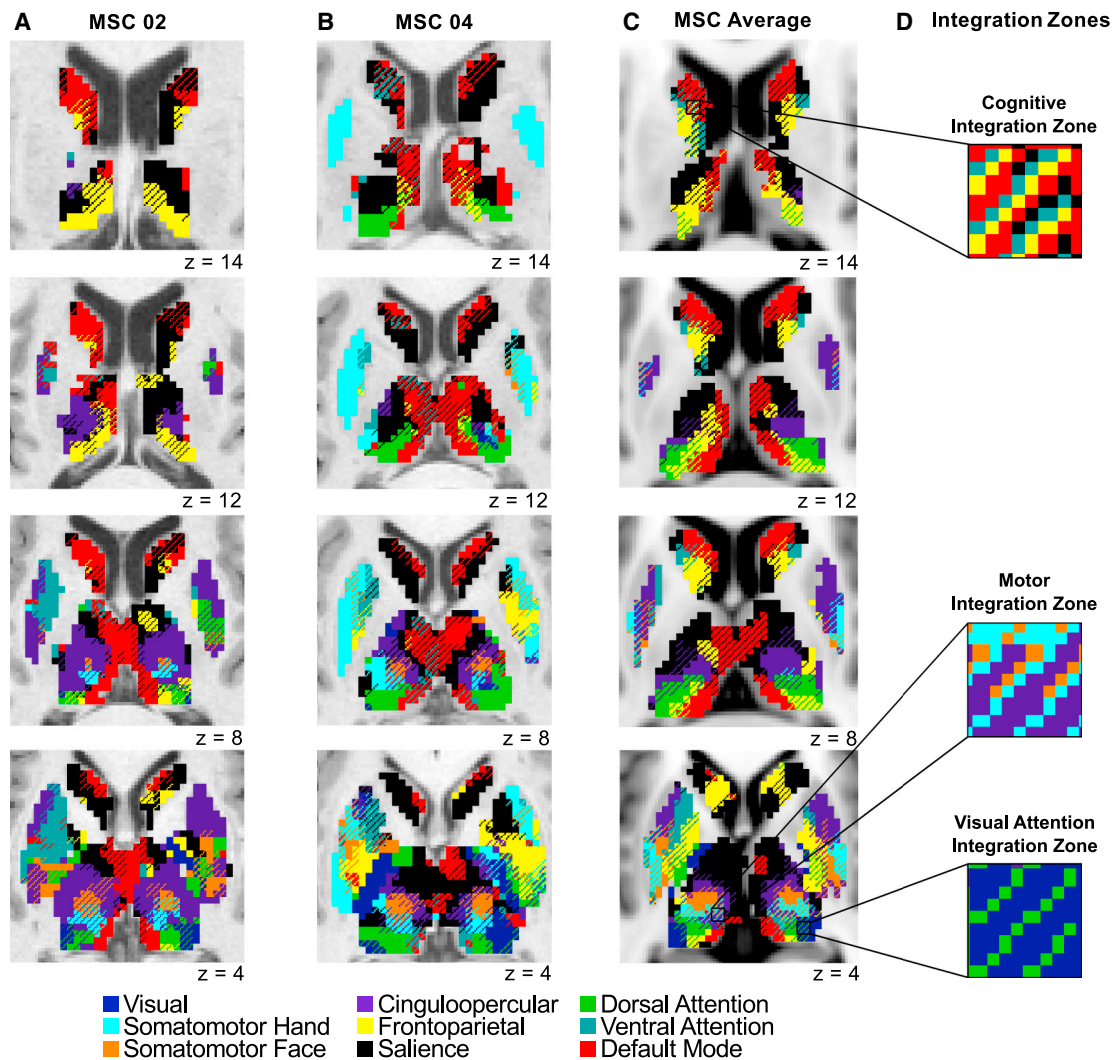
Figure 3. Network-Specific and Integrative Functional Zones in the Basal Ganglia and Thalamus

(A–C) Data displayed for (A) one male representative subject (MSC02), (B) one female representative subject (MSC04), and (C) the group average (all subjects are shown in Figure S7). Voxels with preferential RSFC to one network (network-specific) are represented by solid colors, and voxels functionally connected to multiple networks (integrative) are represented by cross-hatching. Anatomical left is image left.

(D) Zooming in on several integration zones (three distinct clusters of integration zones; see Figure 5): cognitive integration zones, motor integration zones, and visual attention integration zones.

disproportionately biased to be defined as integrative). We found that subcortical integrative voxels were not substantially altered by differences in the number of *a priori* cortical networks (Figure S8). The percent of integrative voxels (45% reported above) was 40% when using the 7-network Infomap solution and 48% when using the 15-network Infomap solution. Community density analyses support the idea that integration was not driven by proximity to more networks because an average of 46% of voxels with a community density of more than 1 were defined as integrative (range, 35%–57% across subjects). Thus, high community density did not bias whether a voxel was defined as integrative or network-specific.

Further, the higher-resolution (2.6 mm) data collected from MSC06 confirmed the presence of integrative voxels in the

subcortex, suggesting that integration was not a simple byproduct of mixing signals within 4-mm voxels. Rather, we found a slightly higher percent of subcortical integrative voxels in MSC06 with the higher-resolution data (51% versus 45%) that was largely due to more integrative voxels in the thalamus (62% with 2.6 mm versus 38% with 4 mm). Thus, integration in the thalamus was not related to the resolution of the data.

Three Clusters of Network Integration Are Present in the Subcortex

To determine which networks preferentially integrate with each other, we quantified the number of integrative subcortical voxels for each network-network pair (e.g., the number of voxels integrating frontoparietal and salience networks) summed across
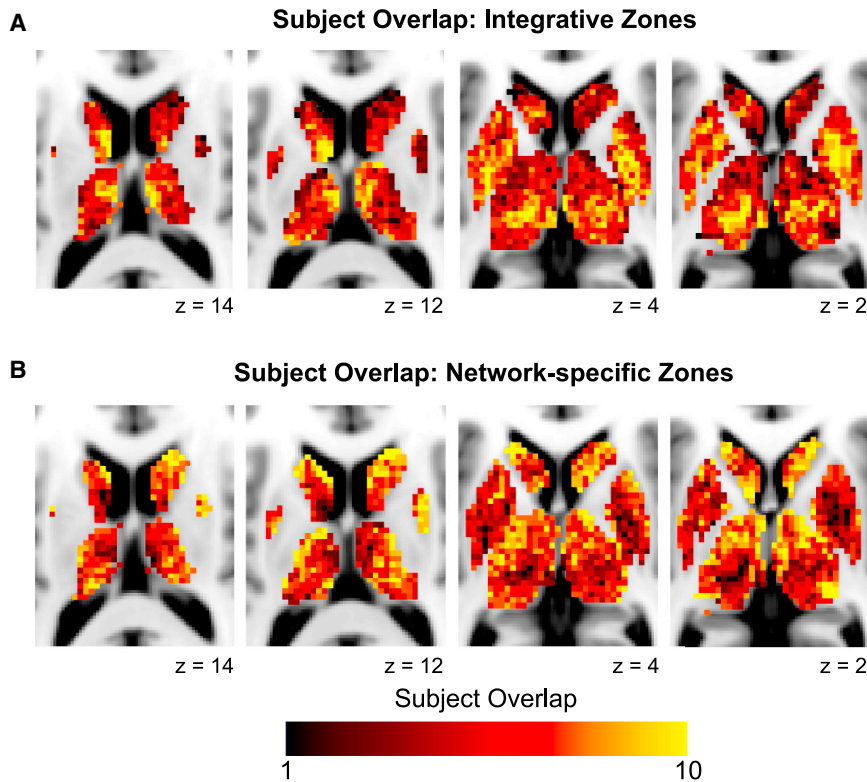
CellPress

A   Subject Overlap: Integrative Zones

z = 14   z = 12   z = 4   z = 2

B   Subject Overlap: Network-specific Zones

z = 14   z = 12   z = 4   z = 2

Subject Overlap

1   10

Figure 4. Overlap across Individuals of Integrative and Network-Specific Functional Zones
(A and B) Higher values represent voxels with (A) integrative functional zones present in multiple subjects and (B) network-specific functional zones present in multiple subjects.

specificity and whether the network(s) functionally connected with these voxels were consistent or variable across individuals. Voxels were considered network-specific when they exhibited strong RSFC to one network only and were considered integrative when they exhibited strong RSFC to more than one network. Voxels were then considered consistent across the group when more than five subjects shared the same network assignment(s); otherwise, they were considered individual-specific. These criteria delineated four types of functional zones in the subcortex: (1) group network-specific zones with consistent network specificity in most subjects, (2) group integrative zones with integration of the same networks in most subjects, (3) individual network-specific zones with variable network specificity across subjects, and (4) individual integrative zones with variable network integration across subjects. To assess confidence in these zone assignments, we implemented a jack-knifing procedure in which the functional zones were assigned as just described ten times, leaving out a unique subject with each iteration. The percent of iterations a given voxel was assigned to a functional zone provides a confidence level for the functional zone assignment and is illustrated in Figure 6A. Variability in signal intensity after nonlinear atlas registration was not related to whether a voxel was identified as group or individual (comparison of signal intensity for group versus individual voxels: $t = 0.65$, $p = 0.52$), suggesting that the network assignment was not significantly related to anatomical alignment.

Figure 6B displays the RSFC profiles of example seed regions in the basal ganglia and thalamus from representative MSC subjects (varies by panel) that exemplify each of the four zones. Group network-specific zones included regions in the medial thalamus with preferential RSFC to the default mode network in most subjects and regions in the head of the caudate with preferential RSFC to the salience network in most subjects. Group integrative zones were primarily located in the ventral intermediate thalamus with integration of cingulo-opercular and somatomotor networks (hand and face) in all ten subjects and in the caudate with integration of control networks. Individual network-specific zones included the head of the caudate with preferential RSFC to the frontoparietal, ventral attention, salience, or default mode networks. These zones were also found in regions of the putamen and dorsal thalamus with
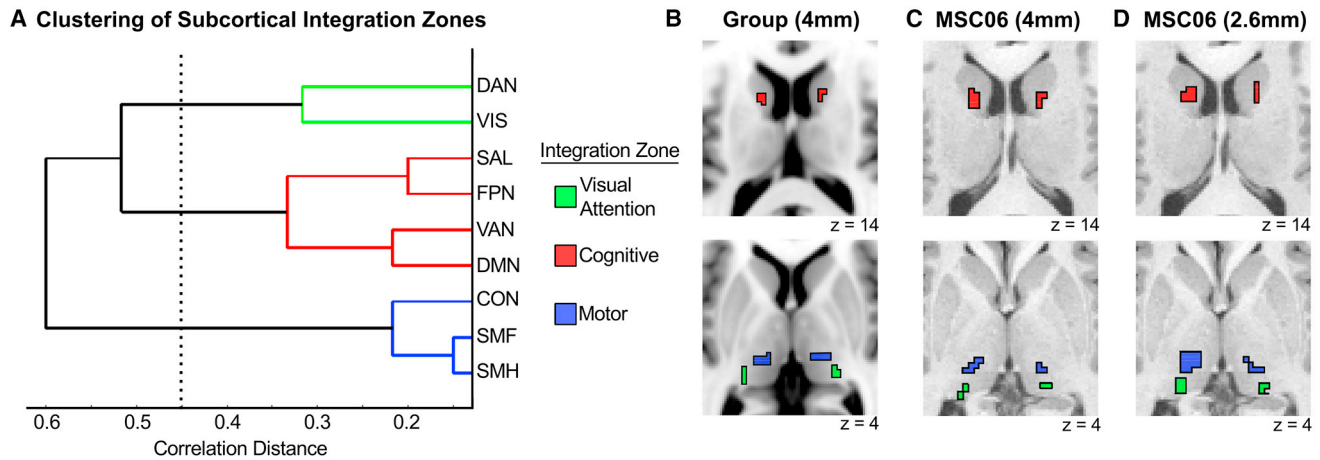
subjects. We normalized these summed values by the total number of integrative voxels, resulting in a percentage of integrative voxels for each network-network pair. This network-by-network matrix was submitted to hierarchical clustering and revealed three clusters of network integration, indicating preferential integration of particular networks (Figure 5A; cophenetic $r = 0.82$).

We found a "motor integration" cluster, which demonstrated integration of the somatomotor hand, somatomotor face, and cingulo-opercular networks. Topographically, this integration was most prominent in the ventral intermediate thalamus (Figure 5B). We also found a "cognitive integration" cluster, which demonstrated preferential integration of the ventral attention, frontoparietal, salience, and default mode networks. Integration of these higher-order networks was most prominent in the caudate (Figure 5B). A third "visual attention integration" cluster included the dorsal attention and visual networks. Integration of these networks was most prominent in the posterior portion of the thalamus (corresponding to the pulvinar; Figure 5B). These three clusters were identified at the individual subject level in both the 4 mm (Figure 5C) and 2.6 mm (Figure 5D) resolution data. This three-cluster solution was replicated using modularity, a graph theoretic clustering algorithm (Newman, 2006).

The Basal Ganglia and Thalamus Contain Four Distinct Types of Functional Zones

Given our framework for understanding cortico-subcortical RSFC (Figure 1), we investigated which basal ganglia and thalamus voxels exhibited properties of integration versus network

Figure 5. Three Clusters of Network Integration Are Present in the Subcortex
(A) Hierarchical clustering revealed three clusters of network integration involving (1) dorsal attention and visual networks; (2) salience, frontoparietal, ventral attention, and default mode networks; and (3) cingulo-opercular, somatomotor face, and somatomotor hand networks.
(B) Most prominent locus of each cluster for the group average.
(C) Most prominent locus of each cluster for an example individual (MSC06) with 4 mm-resolution data.
(D) Most prominent locus of each cluster for the same individual (MSC06) with 2.6 mm-resolution data.

preferential RSFC to the cingulo-opercular, dorsal attention, salience, or somatomotor hand networks. Individual integrative zones were located in portions of the putamen and in the ventral thalamus with variable integration of the default-mode, frontoparietal, ventral attention, salience, cingulo-opercular, and somatomotor networks.
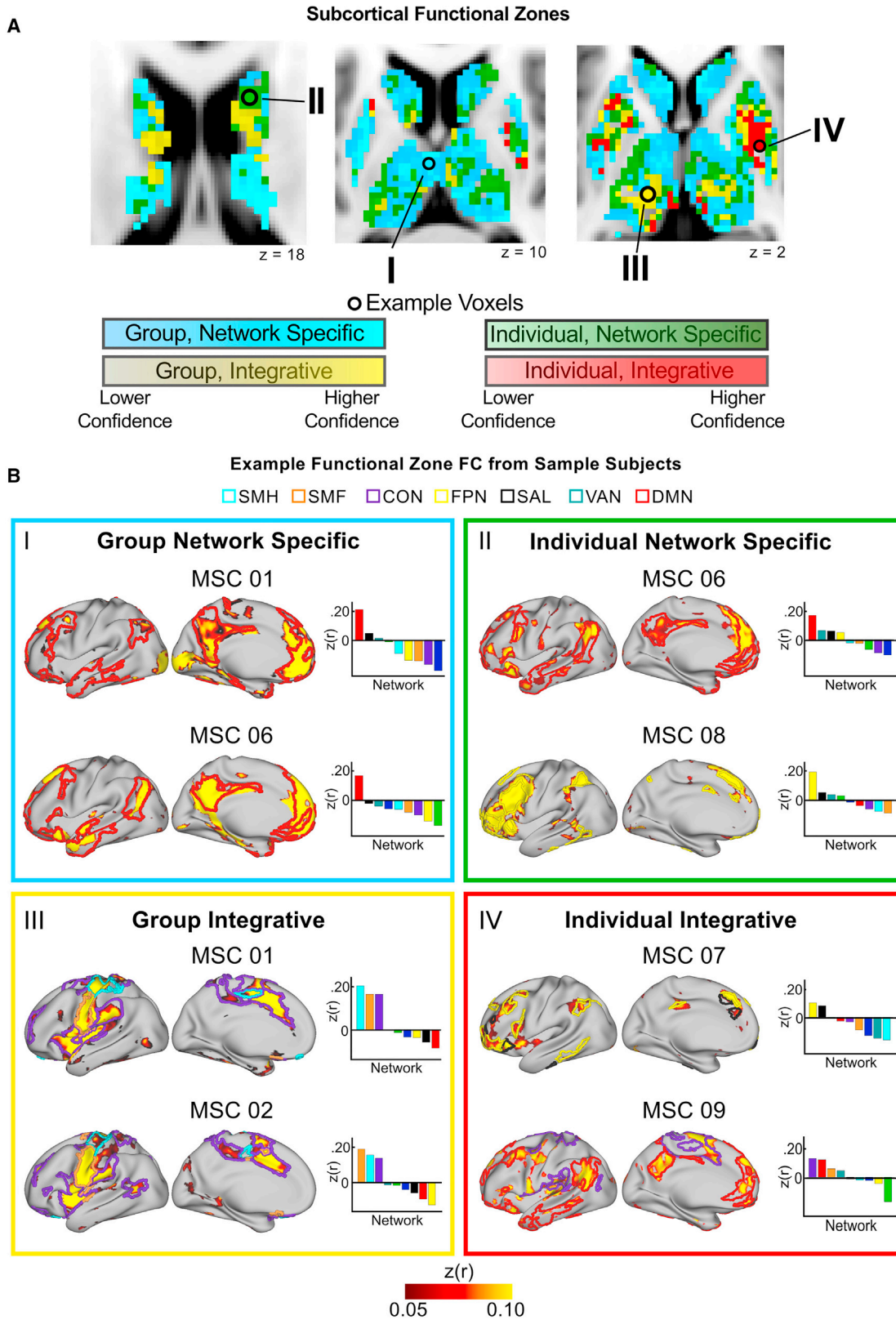
DISCUSSION

We characterized the functional network organization of the human basal ganglia and thalamus at the level of the individual, using PFM with highly sampled, individual subject fMRI data from the MSC dataset. Our analyses revealed distinct zones of network integration (strong functional connectivity with multiple networks) in 45% of the subcortex and network specificity (strong functional connectivity with a single network) in 55% of the subcortex. We also found individual variability in cortico-subcortical RSFC in 43% of the subcortex and commonalities across the group in 57% of the subcortex. Integration zones were found in reliably localizable regions such that the ventral intermediate thalamus integrated cingulo-opercular and somatomotor networks (motor integration zones), the pulvinar integrated dorsal attention and visual networks (visual attention integration zones), and the caudate nucleus integrated default mode and several executive control networks (cognitive integration zones). The motor integration zones were remarkably consistent across all ten individuals, suggesting a vital role for the cingulo-opercular network in top-down control of motor functions. Integration zones were also found in regions of the putamen and pallidum, with individually variable integration of control and somatomotor networks. Overall, the ability to reliably measure cortico-subcortical RSFC in individuals using PFM holds promise for clinical treatments that require precise targeting of subcortical structures, such as DBS.

Individual Specificity and Consistency in Subcortical RSFC Varies by Network

We found individual variability in subcortical RSFC that was not captured by the group average and could only be elucidated by individual-level analyses, in addition to broad similarities across subjects that were captured by the group average. The existence of both individual-specific and shared features is consistent with recent cortical and cerebellar RSFC findings (Gratton et al., 2018; Marek et al., 2018). Given the phylogenetically older origin of the subcortex compared to the cortex (Grillner et al., 2013) and the small size of subcortical structures, one might have expected less individual variability in the subcortex, but we found strong individual-level contributions.

Interestingly, particular functional networks in the subcortex—salience, frontoparietal, ventral attention, and dorsal attention—were relatively more variable across individuals, whereas others—cingulo-opercular and somatomotor—were more consistent. Recent studies have suggested that, in the cortex, networks supporting top-down control show greater individual differences than other networks (Finn et al., 2015; Gratton et al., 2018; Horien et al., 2019; Laumann et al., 2015; Miranda-Dominguez et al., 2014; Mueller et al., 2013). It is notable that the cingulo-opercular network, an executive control network (Crittenden et al., 2016; Duncan and Owen, 2000; Nelson et al., 2010; Neta et al., 2015; Sadaghiani and D'Esposito, 2015), was relatively more stable across individuals in the subcortex. Thus, it stands as an intriguing exception to the more individually variable control networks (see below for further discussion). Further investigation using larger cohorts of highly sampled, individual-specific datasets will help elucidate how these differences in individual variability across networks relate to individual differences in behavior.

A Subcortical Functional Zones

z = 18   z = 10   z = 2

II   I   III   IV

○ Example Voxels

Group, Network Specific
Group, Integrative
Lower Confidence   Higher Confidence

Individual, Network Specific
Individual, Integrative
Lower Confidence   Higher Confidence

B Example Functional Zone FC from Sample Subjects

□SMH □SMF □CON □FPN □SAL □VAN □DMN

I **Group Network Specific**
MSC 01
MSC 06

II **Individual Network Specific**
MSC 06
MSC 08

III **Group Integrative**
MSC 01
MSC 02

IV **Individual Integrative**
MSC 07
MSC 09

z(r)
0.05   0.10

(legend on next page)

PFM Differentiates Four Types of Subcortical Functional Zones

Our individual-specific approach identified four types of functional zones within subcortical structures: group network-specific, group integrative, individual network-specific, and individual integrative. Distinguishing these functional zones is possible only by obtaining individual-level results. Functional parcellation of subcortical structures in individuals has been conducted with conventional quantities of resting-state fMRI data (5–20 min per subject; Garcia-Garcia et al., 2018; Janssen et al., 2015). However, the methods employed in these studies relied on a group-average reference and clustering algorithms within small structures, which are susceptible to bias because of spatial autocorrelation. Further, we show that 100 min or more are needed to reliably estimate individual cortico-subcortical RSFC in some structures (globus pallidus, thalamus). Thus, with the high reliability afforded by PFM, we were able to identify functional zones beyond broad subdivisions of the subcortex in individuals. Indeed, more data were required to obtain reliable estimates in the subcortex compared to the cortex, which may be due to biological differences between structures that affect BOLD signal properties or due to methodological differences, such as distance from the MRI head coil, susceptibility artifacts, and/or reduced gray-white contrast.

The Subcortex Contains Sites of Functional Network Integration and Specificity

We provide compelling human *in vivo* evidence for the existence of network-specific and integrative zones in subcortical structures, consistent with animal models of parallel and integrative cortico-subcortical circuits (Averbeck et al., 2014; Haber, 2003, 2016). The presence of both network-specific and integrative functional zones in the subcortex may be critical for coordinating behavior that requires interactions between functions subserved by distinct functional networks, depending on the demands of the environment (Haber, 2003). That is, certain behavioral contexts may require independent functioning of a specific network, whereas others may require behavior that involves coordination of multiple network functions.

Previous human neuroimaging studies that discussed convergence zones or hubs within the basal ganglia and thalamus did not consider the functional network organization of the brain and/or necessarily relied upon group averaging (Choi et al., 2017; Draganski et al., 2008; Hwang et al., 2017; Jarbo and Verstynen, 2015), both of which could lead to the appearance of integration artifactually. For example, apparent integration of anatomically defined frontal and parietal regions may simply reflect the anatomically distributed organization of the frontoparietal network rather than integration of multiple networks. In addition, group averaging may create the spurious

appearance of integration because brain organization is spatially variable, and, thus, the same brain stereotactic location may be linked to different networks in different individuals (Argall et al., 2006; Laumann et al., 2015; Van Essen, 2005). If a particular location is connected to different networks in different individuals, averaging those signals across the group can result in a signal correlated with multiple networks, even if this "integration" is not present in individual subjects. Consequently, mapping zones of integration must be done at the level of the individual.

Our results are in line with existing evidence from structural (Draganski et al., 2008; Jarbo and Verstynen, 2015) and functional connectivity studies (Garrett et al., 2018; Hwang et al., 2017) that suggest that the basal ganglia and thalamus play central roles in the functional integration of cortical networks. One way in which this integration may occur is via cortico-striato-thalamo-cortical loops. Specifically, cortical inputs are integrated within the basal ganglia and thalamus before being projected diffusely to multiple cortical networks (Alexander et al., 1986; Averbeck et al., 2014; Draganski et al., 2008; Jarbo and Verstynen, 2015; Jones, 1998; Metzger et al., 2013). Thus, the basal ganglia and thalamus simultaneously receive and integrate signals from the cortex and transmit signals to multiple cortical functional networks (Bosch-Bouju et al., 2013; Jones, 1998). Our results provide corroborating evidence that specific focal regions of the subcortex are functionally connected to multiple cortical networks.

From fMRI data, we cannot determine whether functional integration in the subcortex reflects direct convergence of projections to and from multiple cortical networks or interdigitated projections at the neuronal level. Animal research suggests that overlap of terminal fields reflects interdigitated projections (Selemon and Goldman-Rakic, 1985), but further investigation is needed. Our results can inform future animal work by guiding particular anatomical targets of study. For example, integration zones that are common across subjects – e.g., motor integration zones in the thalamus – may be particularly good candidates for investigating projections at the neuronal level. Although the definition of integration zones could be influenced by our methods, we showed consistent results across multiple approaches for defining integrative voxels (Figure S6). Further, we corroborated these integration zones with higher-resolution (2.6 mm) data (Figure 5), which showed even greater integration in the thalamus than with 4 mm data.

In addition, it is important to note that the cortico-subcortical RSFC analyses presented here did not account for connectivity within the subcortex (e.g., thalamo-striatal connections). Future methods that can account for both subcortico-

Figure 6. The Subcortex Contains Four Distinct Functional Zones: Group Network-Specific, Group Integrative, Individual Network-Specific, and Individual Integrative
(A) Anatomical distribution of each functional zone. Color gradation displays the confidence of zone assignment for each voxel, as estimated by a jack-knifing procedure.
(B) Typical examples of each type of functional zone using "example voxels" from (A). Colored borders on the cortical surface represent the outline of the individual's cortical networks that show strong RSFC with the example voxel. Bar graphs display RSFC correlations between the example voxel and each cortical network.
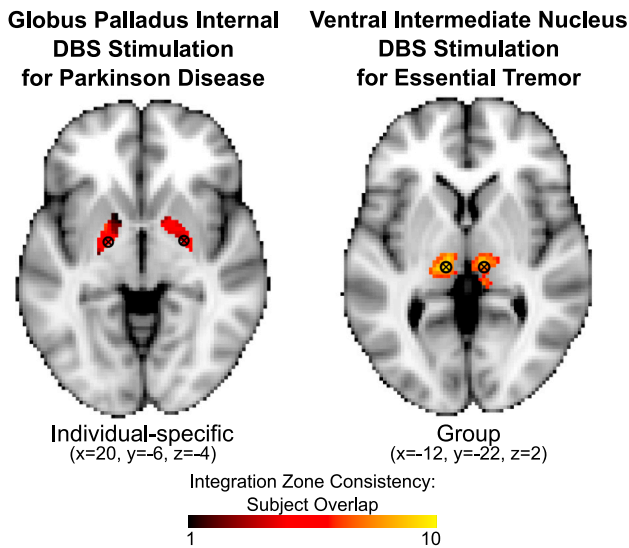
Figure 7. Overlap of Integration Zones and Common Sites of DBS
Sites of DBS are shown, with commonly targeted coordinates overlaid onto individual-specific (globus pallidus) and group (ventral intermediate thalamus) functional zones from the present study. Color gradation shows the consistency of the integration zones across subjects. The globus pallidus site, which has variable success rates, overlaps with an individual integration zone. The ventral intermediate thalamus site, which has consistently high success rates, overlaps with a group integration zone.

subcortical and cortico-subcortical connections may provide further insight into functional network integration within the subcortex.

Functional Networks Preferentially Converge in Focal Regions of the Subcortex

With the precision afforded by PFM, we were able to delineate specific regions within subcortical structures that integrated multiple networks. These integration zones were found with standard (4 mm) as well as high-resolution (2.6 mm) fMRI data. They may serve as critical hubs connecting cortical functional networks via cortico-striato-thalamo-cortical loops. Most studies investigating functional network hubs, including our own, have largely ignored or de-emphasized subcortical structures (e.g., He and Evans, 2010; Power et al., 2011, 2013; Yeo et al., 2011). However, it is possible that hubs critical for information flow between cortical networks are located in the subcortex. The integration zones described here reflect the precise location of putative subcortical hubs and the specific functional networks that converge within them. Three types of integration zones with distinct preferential connectivity emerged: motor integration zones, visual attention integration zones, and cognitive integrations zones.

Motor Integration Zones

The integration zones that were consistently present in all ten individuals combined the somatomotor hand, somatomotor face, and cingulo-opercular networks in the ventral intermediate portion of the thalamus. Thalamic integration of these networks suggests that the cingulo-opercular network might exert some level of control over motor outputs via the thalamus. The current dominantly held view is that the cingulo-opercular network is involved in sustained aspects of task control (Crittenden et al., 2016; Dosenbach et al., 2006, 2007, 2008; Duncan and Owen, 2000; Sadaghiani and D'Esposito, 2015). The cingulo-opercular network has properties similar to other controls networks (e.g., frontoparietal, salience), such as cue activations and error monitoring (Dosenbach et al., 2007; Neta et al., 2015; Petersen and Posner, 2012), that are distinct from lower-level processing networks (e.g., somatomotor networks). However, there is some evidence that a subset of cingulo-opercular regions in the cortex, unlike other control networks, link to somatomotor networks (Gordon et al., 2018; Power et al., 2011) and show activity corresponding to the moment a response is made (Gratton et al., 2017). Non-human primate studies have identified "cingulate motor areas" that play a role in motor planning, preparation, and execution (Dum and Strick, 1993). Further, data from stroke patients suggest that some cingulo-opercular regions are necessary for executing motor functions (Rinne et al., 2018). Interestingly, functional connectivity between the cingulo-opercular and somatomotor networks increases with development in a manner that suggests maturation of inhibitory control (Marek et al., 2015). Thus, the cingulo-opercular network appears to be linked to somatomotor networks in a way that is distinct from other control networks. Our results indicate that the ventral intermediate region of the thalamus may be a critical locus of this integration.

Visual Attention Integration Zones

In the posterior thalamus, corresponding to the location of the pulvinar, we observed preferential integration of the dorsal attention and visual networks. Previous work in non-human primates has shown that the pulvinar is involved in attentional selection and in regulating the transmission of information across the visual cortex (Petersen et al., 1985, 1987; Saalmann et al., 2012). Human fMRI data also support a role for the pulvinar in attentional filtering of irrelevant information (Fischer and Whitney, 2012). Here we show that the pulvinar is a site of integration of the visual network, which comprises primary and association visual areas, and the dorsal attention network, which comprises posterior parietal cortex and frontal eye fields and is involved in spatial attention (Corbetta and Shulman, 2002). Diffusion imaging in humans and anatomical tracing studies in nonhuman primates support this notion of integration. Specifically, structural connections exist between the pulvinar and primary and association visual cortex. Projections from the frontal eye fields and intraparietal sulcus indirectly innervate the pulvinar via ascending projections from the superior colliculus, forming cortico-colliculo-pulvino-cortical loops (Leh et al., 2008; Shipp, 2001, 2004; Weller et al., 2002). These structurally and functionally integrative connections of the pulvinar suggest that it may operate by coordinating attentional functions via integration of the visual and dorsal attention networks (Kastner and Pinsk, 2004; Shipp, 2004).

Cognitive Integration Zones

Particular networks supporting top-down control and attention (fronto-parietal, salience, ventral attention) and the default mode network showed preferential integration in certain regions of the subcortex. Integration zones in the caudate and dorsal
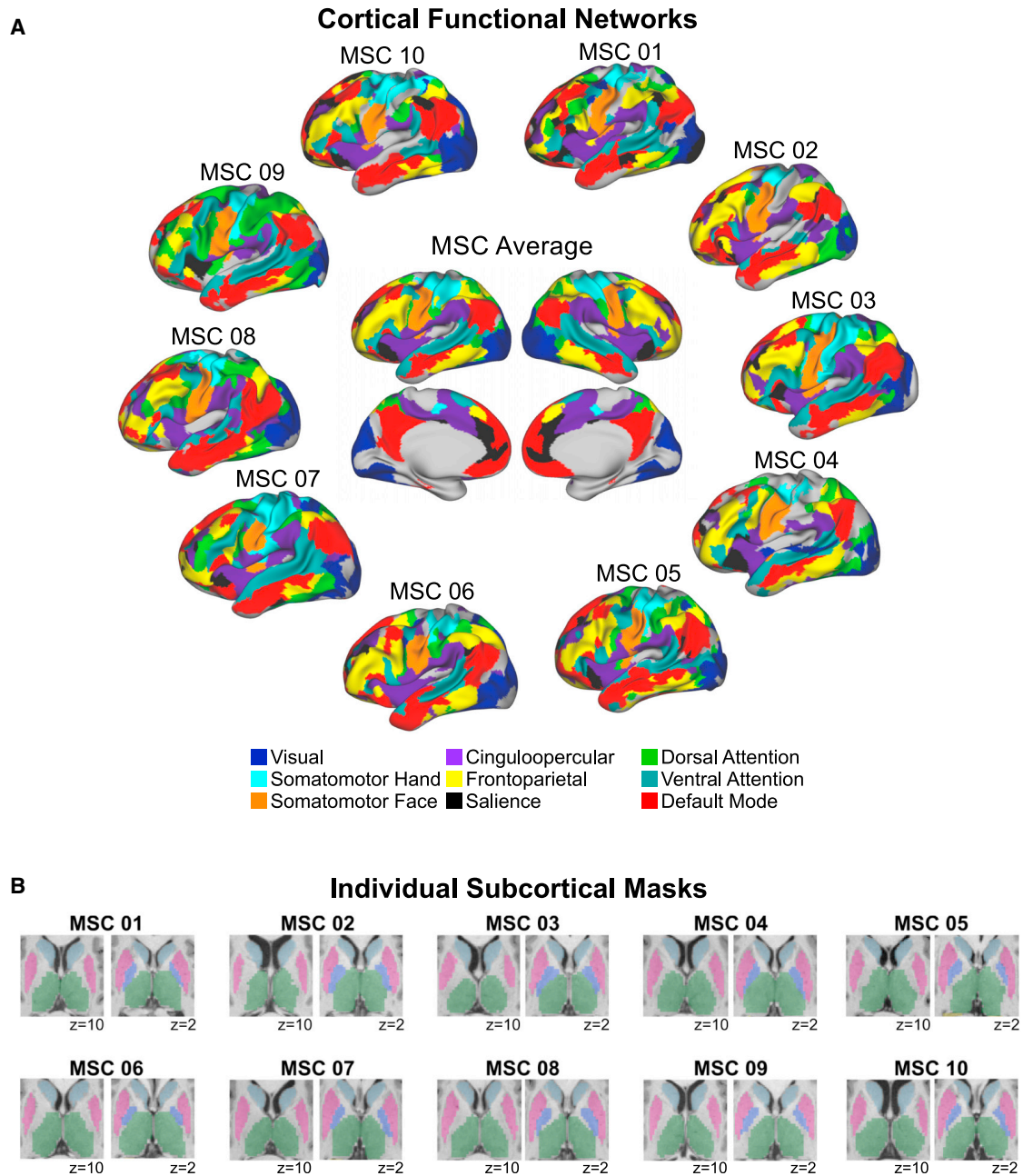
CellPress

Figure 8. Functional Cortical Networks and Subcortical Voxels for Each Individual
(A) Individually defined functional networks (defined as in Gordon et al., 2017b) and the group average functional networks are shown. Nine previously well-characterized functional networks were selected to investigate cortico-subcortical functional connectivity involving cortical networks that are described consistently using different methods and by multiple investigator groups (e.g., Damoiseaux et al., 2006; Gordon et al., 2016; Power et al., 2011; Yeo et al., 2011). Uncolored regions correspond to vertices that were not part of these nine networks according to the Infomap network assignments. Note that including all 15 Infomap networks (excluding unassigned and medial temporal vertices) did not change the results.
(B) Subcortical masks from Freesurfer, edited manually using Freeview, are shown for each individual. Light blue, caudate; pink, putamen; violet, pallidum; green, thalamus.

thalamus exhibited a similar convergence of networks across individuals, whereas integration zones in the putamen and pallidum exhibited individually variable convergence of these networks. The zones in the caudate overlap substantially with

non-human primate studies showing converging projections from widespread areas of the frontal lobe, including the ventromedial prefrontal cortex (PFC), anterior cingulate cortex, ventrolateral PFC, and dorsal PFC (Averbeck et al., 2014). These

CellPress

regions are part of the default mode (ventromedial PFC), salience (anterior cingulate cortex), ventral attention (ventrolateral PFC), and frontoparietal (dorsal PFC) networks. Similarly, in the dorsal thalamus, non-invasive diffusion studies in humans show structural connectivity to widespread areas of the PFC (Behrens et al., 2003). Together, our results suggest that these regions may act to functionally integrate control and default mode networks similarly across individuals in the caudate and dorsal thalamus but variably across individuals in the putamen and pallidum.

Clinical Importance of Subcortical Functional Integration Zones

Given the involvement of cortico-subcortical circuits in many neurological and psychiatric disorders (Albin et al., 1989; Bradshaw and Sheppard, 2000; Drysdale et al., 2017; Greene et al., 2017; Liston et al., 2011; Mink, 2003), the functional integration zones we uncovered may be hotspots for neurological and psychiatric morbidity. Zones with common profiles across individuals may be affected similarly across disorders, whereas zones with variable profiles across individuals may be important for understanding heterogeneity across and within specific disorders. It is also possible that integration zones may be more affected in psychopathology than network-specific zones, relating to the complex nature of many neuropsychiatric disorders. One might expect that the impairments often seen across multiple functional domains (motor, cognitive, affective) in many disorders (Heller, 2016; Luking et al., 2016; Ring and Serra-Mestres, 2002) are more likely the result of alterations to integration zones, whereas alterations to network-specific zones may only affect one or a few functions. Thus, our results can guide future targets of study, both in understanding the functional role of these zones as well as in understanding how each may be affected (and potentially targeted for treatment) in psychopathology.

Precision Functional Mapping of Subcortical Structures May Guide Targets for DBS

PFM has the potential to improve success of interventions that target subcortical structures, most notably DBS. Presently, it is unclear why certain DBS target sites have more consistent efficacy than others and how stimulation of a given target modulates functional networks to alter behavior and/or clinical outcomes (Alhourani et al., 2015). There is work, primarily in Parkinson disease (PD), investigating the relationship between anatomical locations of stimulation and clinical outcome (reviewed in Horn, 2019). In particular, two recent studies (Bot et al., 2018; Horn et al., 2019) pinpointed a specific subthalamic nucleus location as the best predictor of treatment response in PD. Although promising, this anatomically defined location still only explains 27% of the variance in clinical outcome. Further, there is a high degree of overlap between stereotactic coordinates of responders and non-responders. Thus, better accounts of function and individual neuroanatomical variability may improve the efficacy of DBS and other treatment approaches, such as focused ultrasound (Bot et al., 2018; Horn, 2019; Horn et al., 2019; Nestor et al., 2014; Zaaroor et al., 2018). It has been shown, using typical amounts of functional connectivity data per subject (6–12 min), that stimulation sites reported previously to be effective for the same disease belong to the same functional brain networks (e.g., DBS of the globus pallidus and transcranial magnetic stimulation of the primary motor cortex in PD), highlighting the promise of network-based approaches (Fox et al., 2014). However, these studies did not account for the possibility that individual variability in subcortical organization may influence the consistency of DBS success.

Our results present the compelling possibility that PFM could explain the clinical variability of DBS outcomes and help guide DBS placement in the future (Figure 7). We speculate that PFM could ultimately be used to locate patient-specific nodes of a particular functional network for which stimulation improves symptoms. For example, the DBS sites most commonly targeted for essential tremor fall in the group (i.e., low variability) motor integration zones in the thalamus identified in the present study; DBS sites commonly targeted for PD and dystonia fall in individual-specific (i.e., highly variable) sites in the globus pallidus internal (GPi). Thus, the consistent clinical improvement following stimulation of the ventral intermediate thalamic DBS target (i.e., >80% improvement in all essential tremor patients) (Perlmutter and Mink, 2006) may reflect the highly consistent location of the motor integration zones across individuals. By contrast, the GPi location targeted for PD and dystonia varies in its functional connectivity across subjects. This finding may account for the increased variability in clinical outcomes (Campbell et al., 2008, 2012; Hershey et al., 2010; Houeto et al., 2003; Mandat et al., 2006; Perriol et al., 2006; Starr et al., 2006; Wodarg et al., 2012) and the lack of ability to identify optimal stimulation regions within the GPi target in group-level studies of DBS outcomes (Nestor et al., 2014; Tolleson et al., 2015). Perhaps there is a relationship between the clinical response rate to GPi DBS and a particular functional connectivity pattern at the stimulation site. If DBS in PD and dystonia were able to consistently target the same functional network(s), then clinical outcomes might improve considerably. Examining the relationships between the target functional zones identified in the present study and clinical DBS outcomes is an exciting avenue of future research with the potential to inform clinical care.

STAR★METHODS

Detailed methods are provided in the online version of this paper and include the following:

- KEY RESOURCES TABLE
- LEAD CONTACT AND MATERIALS AVAILABILITY
- EXPERIMENTAL MODEL AND SUBJECT DETAILS
  - Participants and Study Design
- METHOD DETAILS
  - MRI image acquisition
- QUANTIFICATION AND STATISTICAL ANALYSIS
  - MRI Data Processing and Surface Registration
  - Structural MRI
  - Functional MRI preprocessing
  - Functional connectivity preprocessing
  - Component-based nuisance regression
  - Analysis Overview
- DATA AND CODE AVAILABILITY

CellPress

SUPPLEMENTAL INFORMATION

ACKNOWLEDGMENTS

AUTHOR CONTRIBUTIONS

Conceptualization, D.J.G., S.M., E.M.G., J.S.S., J.L.R., S.A.N., and N.U.F.D.; Methodology, Software, and Formal Analysis, D.J.G., S.M., E.M.G., J.S.S., C.G., T.O.L., D.D., A.N.V., M.O., D.J.N., A.Z.S., B.L.S., S.E.P., and N.U.F.D.; Investigation, Resources, and Data Curation, D.J.G., M.O., T.O.L., A.W.G., J.J.B., A.L.N., D.J.N., J.M.H., A.N.N., K.B.M., S.M.N., and N.U.F.D.; Writing – Original Draft, D.J.G., S.M., S.A.N., and N.U.F.D.; Writing – Review & Editing, D.J.G., S.M., E.M.G., J.S.S., C.G., T.O.L., A.W.G., J.J.B., A.L.N., D.D., A.N.V., M.O., D.J.N., J.M.H., A.N.N., K.B.M., J.L.R., S.A.N., S.M.N., A.Z.S., B.L.S., S.E.P., and N.U.F.D.; Supervision, D.J.G. and N.U.F.D.

DECLARATION OF INTERESTS

The authors declare no competing interests.

REFERENCES

Albin, R.L., Young, A.B., and Penney, J.B. (1989). The functional anatomy of basal ganglia disorders. Trends Neurosci. 12, 366–375.

Alexander, G.E., and Crutcher, M.D. (1990). Functional architecture of basal ganglia circuits: neural substrates of parallel processing. Trends Neurosci. 13, 266–271.

Alexander, G.E., DeLong, M.R., and Strick, P.L. (1986). Parallel organization of functionally segregated circuits linking basal ganglia and cortex. Annu. Rev. Neurosci. 9, 357–381.

Alexander, G.E., Crutcher, M.D., and DeLong, M.R. (1990). Basal ganglia-thalamocortical circuits: parallel substrates for motor, oculomotor, "prefrontal" and "limbic" functions. Prog. Brain Res. 85, 119–146.

Alhourani, A., McDowell, M.M., Randazzo, M.J., Wozny, T.A., Kondylis, E.D., Lipski, W.J., Beck, S., Karp, J.F., Ghuman, A.S., and Richardson, R.M. (2015). Network effects of deep brain stimulation. J. Neurophysiol. 114, 2105–2117.

Argall, B.D., Saad, Z.S., and Beauchamp, M.S. (2006). Simplified intersubject averaging on the cortical surface using SUMA. Hum. Brain Mapp. 27, 14–27.

Arsalidou, M., Duerden, E.G., and Taylor, M.J. (2013). The centre of the brain: topographic model of motor, cognitive, affective, and somatosensory functions of the basal ganglia. Hum. Brain Mapp. 34, 3031–3054.

Averbeck, B.B., Lehman, J., Jacobson, M., and Haber, S.N. (2014). Estimates of projection overlap and zones of convergence within frontal-striatal circuits. J. Neurosci. 34, 9497–9505.

Baizabal-Carvallo, J.F., Kagnoff, M.N., Jimenez-Shahed, J., Fekete, R., and Jankovic, J. (2014). The safety and efficacy of thalamic deep brain stimulation in essential tremor: 10 years and beyond. J. Neurol. Neurosurg. Psychiatry 85, 567–572.

Balota, D.A., Yap, M.J., Cortese, M.J., Hutchison, K.A., Kessler, B., Loftis, B., Neely, J.H., Nelson, D.L., Simpson, G.B., and Treiman, R. (2007). The English Lexicon Project. Behav. Res. Methods 39, 445–459.

Barch, D.M., Burgess, G.C., Harms, M.P., Petersen, S.E., Schlaggar, B.L., Corbetta, M., Glasser, M.F., Curtiss, S., Dixit, S., Feldt, C., et al.; WU-Minn HCP Consortium (2013). Function in the human connectome: task-fMRI and individual differences in behavior. Neuroimage 80, 169–189.

Barnes, K.A., Cohen, A.L., Power, J.D., Nelson, S.M., Dosenbach, Y.B., Miezin, F.M., Petersen, S.E., and Schlaggar, B.L. (2010). Identifying Basal Ganglia divisions in individuals using resting-state functional connectivity MRI. Front. Syst. Neurosci. 4, 18.

Behrens, T.E., Johansen-Berg, H., Woolrich, M.W., Smith, S.M., Wheeler-Kingshott, C.A., Boulby, P.A., Barker, G.J., Sillery, E.L., Sheehan, K., Ciccarelli, O., et al. (2003). Non-invasive mapping of connections between human thalamus and cortex using diffusion imaging. Nat. Neurosci. 6, 750–757.

Behzadi, Y., Restom, K., Liau, J., and Liu, T.T. (2007). A component based noise correction method (CompCor) for BOLD and perfusion based fMRI. Neuroimage 37, 90–101.

Bogousslavsky, J., Regli, F., and Uske, A. (1988). Thalamic infarcts: clinical syndromes, etiology, and prognosis. Neurology 38, 837–848.

Bosch-Bouju, C., Hyland, B.I., and Parr-Brownlie, L.C. (2013). Motor thalamus integration of cortical, cerebellar and basal ganglia information: implications for normal and parkinsonian conditions. Front. Comput. Neurosci. 7, 163.

Bostan, A.C., and Strick, P.L. (2018). The basal ganglia and the cerebellum: nodes in an integrated network. Nat. Rev. Neurosci. 19, 338–350.

Bot, M., Schuurman, P.R., Odekerken, V.J.J., Verhagen, R., Contarino, F.M., De Bie, R.M.A., and van den Munckhof, P. (2018). Deep brain stimulation for Parkinson's disease: defining the optimal location within the subthalamic nucleus. J. Neurol. Neurosurg. Psychiatry 89, 493–498.

Bradshaw, J.L., and Sheppard, D.M. (2000). The neurodevelopmental frontostriatal disorders: evolutionary adaptiveness and anomalous lateralization. Brain Lang. 73, 297–320.

Braga, R.M., and Buckner, R.L. (2017). Parallel Interdigitated Distributed Networks within the Individual Estimated by Intrinsic Functional Connectivity. Neuron 95, 457–471.e5.

Campbell, M.C., Karimi, M., Weaver, P.M., Wu, J., Perantie, D.C., Golchin, N.A., Tabbal, S.D., Perlmutter, J.S., and Hershey, T. (2008). Neural correlates of STN DBS-induced cognitive variability in Parkinson disease. Neuropsychologia 46, 3162–3169.

Campbell, M.C., Black, K.J., Weaver, P.M., Lugar, H.M., Videen, T.O., Tabbal, S.D., Karimi, M., Perlmutter, J.S., and Hershey, T. (2012). Mood response to deep brain stimulation of the subthalamic nucleus in Parkinson's disease. J. Neuropsychiatry Clin. Neurosci. 24, 28–36.

Choi, E.Y., Yeo, B.T., and Buckner, R.L. (2012). The organization of the human striatum estimated by intrinsic functional connectivity. J. Neurophysiol. 108, 2242–2263.

Choi, E.Y., Tanimura, Y., Vage, P.R., Yates, E.H., and Haber, S.N. (2017). Convergence of prefrontal and parietal anatomical projections in a connectional hub in the striatum. Neuroimage 146, 821–832.

Ciric, R., Wolf, D.H., Power, J.D., Roalf, D.R., Baum, G.L., Ruparel, K., Shinohara, R.T., Elliott, M.A., Eickhoff, S.B., Davatzikos, C., et al. (2017). Benchmarking of participant-level confound regression strategies for the control of motion artifact in studies of functional connectivity. Neuroimage 154, 174–187.

Corbetta, M., and Shulman, G.L. (2002). Control of goal-directed and stimulus-driven attention in the brain. Nat. Rev. Neurosci. 3, 201–215.

Corbetta, M., Ramsey, L., Callejas, A., Baldassarre, A., Hacker, C.D., Siegel, J.S., Astafiev, S.V., Rengachary, J., Zinn, K., Lang, C.E., et al. (2015).

Common behavioral clusters and subcortical anatomy in stroke. Neuron 85, 927–941.

Crittenden, B.M., Mitchell, D.J., and Duncan, J. (2016). Task Encoding across the Multiple Demand Cortex Is Consistent with a Frontoparietal and Cingulo-Opercular Dual Networks Distinction. J. Neurosci. 36, 6147–6155.

Dale, A.M., Fischl, B., and Sereno, M.I. (1999). Cortical surface-based analysis. I. Segmentation and surface reconstruction. Neuroimage 9, 179–194.

Damoiseaux, J.S., Rombouts, S.A., Barkhof, F., Scheltens, P., Stam, C.J., Smith, S.M., and Beckmann, C.F. (2006). Consistent resting-state networks across healthy subjects. Proc. Natl. Acad. Sci. USA 103, 13848–13853.

Dandekar, M.P., Fenoy, A.J., Carvalho, A.F., Soares, J.C., and Quevedo, J. (2018). Deep brain stimulation for treatment-resistant depression: an integrative review of preclinical and clinical findings and translational implications. Mol. Psychiatry 23, 1094–1112.

Di Martino, A., Scheres, A., Margulies, D.S., Kelly, A.M.C., Uddin, L.Q., Shehzad, Z., Biswal, B., Walters, J.R., Castellanos, F.X., and Milham, M.P. (2008). Functional connectivity of human striatum: a resting state FMRI study. Cereb. Cortex 18, 2735–2747.

Dosenbach, N.U.F., Visscher, K.M., Palmer, E.D., Miezin, F.M., Wenger, K.K., Kang, H.C., Burgund, E.D., Grimes, A.L., Schlaggar, B.L., and Petersen, S.E. (2006). A core system for the implementation of task sets. Neuron 50, 799–812.

Dosenbach, N.U.F., Fair, D.A., Miezin, F.M., Cohen, A.L., Wenger, K.K., Dosenbach, R.A.T., Fox, M.D., Snyder, A.Z., Vincent, J.L., Raichle, M.E., et al. (2007). Distinct brain networks for adaptive and stable task control in humans. Proc. Natl. Acad. Sci. USA 104, 11073–11078.

Dosenbach, N.U.F., Fair, D.A., Cohen, A.L., Schlaggar, B.L., and Petersen, S.E. (2008). A dual-networks architecture of top-down control. Trends Cogn. Sci. 12, 99–105.

Draganski, B., Kherif, F., Klöppel, S., Cook, P.A., Alexander, D.C., Parker, G.J., Deichmann, R., Ashburner, J., and Frackowiak, R.S. (2008). Evidence for segregated and integrative connectivity patterns in the human Basal Ganglia. J. Neurosci. 28, 7143–7152.

Drysdale, A.T., Grosenick, L., Downar, J., Dunlop, K., Mansouri, F., Meng, Y., Fetcho, R.N., Zebley, B., Oathes, D.J., Etkin, A., et al. (2017). Resting-state connectivity biomarkers define neurophysiological subtypes of depression. Nat. Med. 23, 28–38.

Dubis, J.W., Siegel, J.S., Neta, M., Visscher, K.M., and Petersen, S.E. (2016). Tasks Driven by Perceptual Information Do Not Recruit Sustained BOLD Activity in Cingulo-Opercular Regions. Cereb. Cortex 26, 192–201.

Dum, R.P., and Strick, P.L. (1993). Cingulate motor areas. In Neurobiology of cingulate cortex and limbic thalamus: a comprehensive handbook, B.A. Vogt and M. Gabriel, eds. (Boston, MA: Birkhauser), pp. 415–441.

Duncan, J., and Owen, A.M. (2000). Common regions of the human frontal lobe recruited by diverse cognitive demands. Trends Neurosci. 23, 475–483.

Fair, D.A., Bathula, D., Mills, K.L., Dias, T.G., Blythe, M.S., Zhang, D., Snyder, A.Z., Raichle, M.E., Stevens, A.A., Nigg, J.T., and Nagel, B.J. (2010). Maturing thalamocortical functional connectivity across development. Front. Syst. Neurosci. 4, 10.

Filevich, E., Lisofsky, N., Becker, M., Butler, O., Lochstet, M., Martensson, J., Wenger, E., Lindenberger, U., and Kühn, S. (2017). Day2day: investigating daily variability of magnetic resonance imaging measures over half a year. BMC Neurosci. 18, 65.

Finn, E.S., Shen, X., Scheinost, D., Rosenberg, M.D., Huang, J., Chun, M.M., Papademetris, X., and Constable, R.T. (2015). Functional connectome fingerprinting: identifying individuals using patterns of brain connectivity. Nat. Neurosci. 18, 1664–1671.

Fischer, J., and Whitney, D. (2012). Attention gates visual coding in the human pulvinar. Nat. Commun. 3, 1051.

Fischl, B. (2012). FreeSurfer. Neuroimage 62, 774–781.

Fischl, B., Sereno, M.I., and Dale, A.M. (1999). Cortical surface-based analysis. II: Inflation, flattening, and a surface-based coordinate system. Neuroimage 9, 195–207.

Fox, M.D., Buckner, R.L., Liu, H., Chakravarty, M.M., Lozano, A.M., and Pascual-Leone, A. (2014). Resting-state networks link invasive and noninvasive brain stimulation across diverse psychiatric and neurological diseases. Proc. Natl. Acad. Sci. USA 111, E4367–E4375.

Friston, K.J., Williams, S., Howard, R., Frackowiak, R.S., and Turner, R. (1996). Movement-related effects in fMRI time-series. Magn. Reson. Med. 35, 346–355.

Garcia-Garcia, M., Nikolaidis, A., Bellec, P., Craddock, R.C., Cheung, B., Castellanos, F.X., and Milham, M.P. (2018). Detecting stable individual differences in the functional organization of the human basal ganglia. Neuroimage 170, 68–82.

Garrett, D.D., Epp, S.M., Perry, A., and Lindenberger, U. (2018). Local temporal variability reflects functional integration in the human brain. Neuroimage 183, 776–787.

Glass, L. (1969). Moiré effect from random dots. Nature 223, 578–580.

Glasser, M.F., Coalson, T.S., Robinson, E.C., Hacker, C.D., Harwell, J., Yacoub, E., Ugurbil, K., Andersson, J., Beckmann, C.F., Jenkinson, M., et al. (2016). A multi-modal parcellation of human cerebral cortex. Nature 536, 171–178.

Gordon, E.M., Laumann, T.O., Adeyemo, B., Huckins, J.F., Kelley, W.M., and Petersen, S.E. (2016). Generation and Evaluation of a Cortical Area Parcellation from Resting-State Correlations. Cereb. Cortex 26, 288–303.

Gordon, E.M., Laumann, T.O., Adeyemo, B., Gilmore, A.W., Nelson, S.M., Dosenbach, N.U.F., and Petersen, S.E. (2017a). Individual-specific features of brain systems identified with resting state functional correlations. Neuroimage 146, 918–939.

Gordon, E.M., Laumann, T.O., Gilmore, A.W., Newbold, D.J., Greene, D.J., Berg, J.J., Ortega, M., Hoyt-Drazen, C., Gratton, C., Sun, H., et al. (2017b). Precision Functional Mapping of Individual Human Brains. Neuron 95, 791–807.e7.

Gordon, E.M., Lynch, C.J., Gratton, C., Laumann, T.O., Gilmore, A.W., Greene, D.J., Ortega, M., Nguyen, A.L., Schlaggar, B.L., Petersen, S.E., et al. (2018). Three Distinct Sets of Connector Hubs Integrate Human Brain Function. Cell Rep. 24, 1687–1695.e4.

Gratton, C., Neta, M., Sun, H., Ploran, E.J., Schlaggar, B.L., Wheeler, M.E., Petersen, S.E., and Nelson, S.M. (2017). Distinct Stages of Moment-to-Moment Processing in the Cinguloopercular and Frontoparietal Networks. Cereb. Cortex 27, 2403–2417.

Gratton, C., Laumann, T.O., Nielsen, A.N., Greene, D.J., Gordon, E.M., Gilmore, A.W., Nelson, S.M., Coalson, R.S., Snyder, A.Z., Schlaggar, B.L., et al. (2018). Functional Brain Networks Are Dominated by Stable Group and Individual Factors, Not Cognitive or Daily Variation. Neuron 98, 439–452.e5.

Greene, D.J., Laumann, T.O., Dubis, J.W., Ihnen, S.K., Neta, M., Power, J.D., Pruett, J.R., Jr., Black, K.J., and Schlaggar, B.L. (2014). Developmental changes in the organization of functional connections between the basal ganglia and cerebral cortex. J. Neurosci. 34, 5842–5854.

Greene, D.J., Williams Iii, A.C., Koller, J.M., Schlaggar, B.L., and Black, K.J.; The Tourette Association of America Neuroimaging Consortium (2017). Brain structure in pediatric Tourette syndrome. Mol. Psychiatry 22, 972–980.

Grillner, S., Robertson, B., and Stephenson-Jones, M. (2013). The evolutionary origin of the vertebrate basal ganglia and its role in action selection. J. Physiol. 591, 5425–5431.

Haber, S.N. (2003). The primate basal ganglia: parallel and integrative networks. J. Chem. Neuroanat. 26, 317–330.

Haber, S.N. (2016). Corticostriatal circuitry. Dialogues Clin. Neurosci. 18, 7–21.

He, Y., and Evans, A. (2010). Graph theoretical modeling of brain connectivity. Curr. Opin. Neurol. 23, 341–350.

Heller, A.S. (2016). Cortical-Subcortical Interactions in Depression: From Animal Models to Human Psychopathology. Front. Syst. Neurosci. 10, 20.

Hershey, T., Campbell, M.C., Videen, T.O., Lugar, H.M., Weaver, P.M., Hartlein, J., Karimi, M., Tabbal, S.D., and Perlmutter, J.S. (2010). Mapping Go-No-Go performance within the subthalamic nucleus region. Brain 133, 3625–3634.

Horien, C., Shen, X., Scheinost, D., and Constable, R.T. (2019). The individual functional connectome is unique and stable over months to years. Neuroimage *189*, 676–687.

Horn, A. (2019). The impact of modern-day neuroimaging on the field of deep brain stimulation. Curr. Opin. Neurol. *32*, 511–520.

Horn, A., Li, N., Dembek, T.A., Kappel, A., Boulay, C., Ewert, S., Tietze, A., Husch, A., Perera, T., Neumann, W.J., et al. (2019). Lead-DBS v2: Towards a comprehensive pipeline for deep brain stimulation imaging. Neuroimage *184*, 293–316.

Houeto, J.L., Mesnage, V., Welter, M.L., Mallet, L., Agid, Y., and Bejjani, B.P. (2003). Subthalamic DBS replaces levodopa in Parkinson's disease: two-year follow-up. Neurology *60*, 154–155, author reply 154–155.

Hwang, K., Bertolero, M.A., Liu, W.B., and D'Esposito, M. (2017). The Human Thalamus Is an Integrative Hub for Functional Brain Networks. J. Neurosci. *37*, 5594–5607.

Janssen, R.J., Jylänki, P., Kessels, R.P., and van Gerven, M.A. (2015). Probabilistic model-based functional parcellation reveals a robust, fine-grained subdivision of the striatum. Neuroimage *119*, 398–405.

Jarbo, K., and Verstynen, T.D. (2015). Converging structural and functional connectivity of orbitofrontal, dorsolateral prefrontal, and posterior parietal cortex in the human striatum. J. Neurosci. *35*, 3865–3878.

Jones, E.G. (1998). Viewpoint: the core and matrix of thalamic organization. Neuroscience *85*, 331–345.

Kastner, S., and Pinsk, M.A. (2004). Visual attention as a multilevel selection process. Cogn. Affect. Behav. Neurosci. *4*, 483–500.

Laumann, T.O., Gordon, E.M., Adeyemo, B., Snyder, A.Z., Joo, S.J., Chen, M.Y., Gilmore, A.W., McDermott, K.B., Nelson, S.M., Dosenbach, N.U., et al. (2015). Functional System and Areal Organization of a Highly Sampled Individual Human Brain. Neuron *87*, 657–670.

Leh, S.E., Chakravarty, M.M., and Ptito, A. (2008). The connectivity of the human pulvinar: a diffusion tensor imaging tractography study. Int. J. Biomed. Imaging *2008*, 789539.

Lehéricy, S., Ducros, M., Van de Moortele, P.F., Francois, C., Thivard, L., Poupon, C., Swindale, N., Ugurbil, K., and Kim, D.S. (2004). Diffusion tensor fiber tracking shows distinct corticostriatal circuits in humans. Ann. Neurol. *55*, 522–529.

Liston, C., Malter Cohen, M., Teslovich, T., Levenson, D., and Casey, B.J. (2011). Atypical prefrontal connectivity in attention-deficit/hyperactivity disorder: pathway to disease or pathological end point? Biol. Psychiatry *69*, 1168–1177.

Luking, K.R., Pagliaccio, D., Luby, J.L., and Barch, D.M. (2016). Reward Processing and Risk for Depression Across Development. Trends Cogn. Sci. *20*, 456–468.

Mandat, T.S., Hurwitz, T., and Honey, C.R. (2006). Hypomania as an adverse effect of subthalamic nucleus stimulation: report of two cases. Acta Neurochir. (Wien) *148*, 895–897, discussion 898.

Marcus, D.S., Harwell, J., Olsen, T., Hodge, M., Glasser, M.F., Prior, F., Jenkinson, M., Laumann, T., Curtiss, S.W., and Van Essen, D.C. (2011). Informatics and data mining tools and strategies for the human connectome project. Front. Neuroinform. *5*, 4.

Marek, S., Hwang, K., Foran, W., Hallquist, M.N., and Luna, B. (2015). The Contribution of Network Organization and Integration to the Development of Cognitive Control. PLoS Biol. *13*, e1002328.

Marek, S., Siegel, J.S., Gordon, E.M., Raut, R.V., Gratton, C., Newbold, D.J., Ortega, M., Laumann, T.O., Adeyemo, B., Miller, D.B., et al. (2018). Spatial and Temporal Organization of the Individual Human Cerebellum. Neuron *100*, 977–993.e7.

McIntyre, C.C., and Hahn, P.J. (2010). Network perspectives on the mechanisms of deep brain stimulation. Neurobiol. Dis. *38*, 329–337.

Metzger, C.D., van der Werf, Y.D., and Walter, M. (2013). Functional mapping of thalamic nuclei and their integration into cortico-striatal-thalamo-cortical loops via ultra-high resolution imaging-from animal anatomy to in vivo imaging in humans. Front. Neurosci. *7*, 24.

Miezin, F.M., Maccotta, L., Ollinger, J.M., Petersen, S.E., and Buckner, R.L. (2000). Characterizing the hemodynamic response: effects of presentation rate, sampling procedure, and the possibility of ordering brain activity based on relative timing. Neuroimage *11*, 735–759.

Mink, J.W. (2001). Basal ganglia dysfunction in Tourette's syndrome: a new hypothesis. Pediatr. Neurol. *25*, 190–198.

Mink, J.W. (2003). The Basal Ganglia and involuntary movements: impaired inhibition of competing motor patterns. Arch. Neurol. *60*, 1365–1368.

Mink, J.W. (2009). Clinical review of DBS for Tourette Syndrome. Front. Biosci. (Elite Ed.) *1*, 72–76.

Miranda-Dominguez, O., Mills, B.D., Carpenter, S.D., Grant, K.A., Kroenke, C.D., Nigg, J.T., and Fair, D.A. (2014). Connectotyping: model based fingerprinting of the functional connectome. PLoS ONE *9*, e111048.

Mueller, S., Wang, D., Fox, M.D., Yeo, B.T., Sepulcre, J., Sabuncu, M.R., Shafee, R., Lu, J., and Liu, H. (2013). Individual variability in functional connectivity architecture of the human brain. Neuron *77*, 586–595.

Nelson, S.M., Dosenbach, N.U., Cohen, A.L., Wheeler, M.E., Schlaggar, B.L., and Petersen, S.E. (2010). Role of the anterior insula in task-level control and focal attention. Brain Struct. Funct. *214*, 669–680.

Nestor, K.A., Jones, J.D., Butson, C.R., Morishita, T., Jacobson, C.E., 4th, Peace, D.A., Chen, D., Foote, K.D., and Okun, M.S. (2014). Coordinate-based lead location does not predict Parkinson's disease deep brain stimulation outcome. PLoS ONE *9*, e93524.

Neta, M., Miezin, F.M., Nelson, S.M., Dubis, J.W., Dosenbach, N.U., Schlaggar, B.L., and Petersen, S.E. (2015). Spatial and temporal characteristics of error-related activity in the human brain. J. Neurosci. *35*, 253–266.

Newman, M.E. (2006). Modularity and community structure in networks. Proc. Natl. Acad. Sci. USA *103*, 8577–8582.

Noble, S., Spann, M.N., Tokoglu, F., Shen, X., Constable, R.T., and Scheinost, D. (2017). Influences on the Test-Retest Reliability of Functional Connectivity MRI and its Relationship with Behavioral Utility. Cereb. Cortex *27*, 5415–5429.

Ollinger, J.M., Corbetta, M., and Shulman, G.L. (2001). Separating processes within a trial in event-related functional MRI II. Analysis. Neuroimage *13*, 218–229.

Ondo, W., Jankovic, J., Schwartz, K., Almaguer, M., and Simpson, R.K. (1998). Unilateral thalamic deep brain stimulation for refractory essential tremor and Parkinson's disease tremor. Neurology *51*, 1063–1069.

Patriat, R., Molloy, E.K., and Birn, R.M. (2015). Using Edge Voxel Information to Improve Motion Regression for rs-fMRI Connectivity Studies. Brain Connect. *5*, 582–595.

Perlmutter, J.S., and Mink, J.W. (2006). Deep brain stimulation. Annu. Rev. Neurosci. *29*, 229–257.

Perriol, M.P., Krystkowiak, P., Defebvre, L., Blond, S., Destée, A., and Dujardin, K. (2006). Stimulation of the subthalamic nucleus in Parkinson's disease: cognitive and affective changes are not linked to the motor outcome. Parkinsonism Relat. Disord. *12*, 205–210.

Petersen, S.E., and Posner, M.I. (2012). The attention system of the human brain: 20 years after. Annu. Rev. Neurosci. *35*, 73–89.

Petersen, S.E., Robinson, D.L., and Keys, W. (1985). Pulvinar nuclei of the behaving rhesus monkey: visual responses and their modulation. J. Neurophysiol. *54*, 867–886.

Petersen, S.E., Robinson, D.L., and Morris, J.D. (1987). Contributions of the pulvinar to visual spatial attention. Neuropsychologia *25* (1A), 97–105.

Poldrack, R.A., Laumann, T.O., Koyejo, O., Gregory, B., Hover, A., Chen, M.Y., Gorgolewski, K.J., Luci, J., Joo, S.J., Boyd, R.L., et al. (2015). Long-term neural and physiological phenotyping of a single human. Nat. Commun. *6*, 8885.

Power, J.D., Cohen, A.L., Nelson, S.M., Wig, G.S., Barnes, K.A., Church, J.A., Vogel, A.C., Laumann, T.O., Miezin, F.M., Schlaggar, B.L., and Petersen, S.E. (2011). Functional network organization of the human brain. Neuron *72*, 665–678.

Power, J.D., Schlaggar, B.L., Lessov-Schlaggar, C.N., and Petersen, S.E. (2013). Evidence for hubs in human functional brain networks. Neuron *79*, 798–813.

Power, J.D., Mitra, A., Laumann, T.O., Snyder, A.Z., Schlaggar, B.L., and Petersen, S.E. (2014). Methods to detect, characterize, and remove motion artifact in resting state fMRI. Neuroimage *84*, 320–341.

Raut, R.V., Mitra, A., Snyder, A.Z., and Raichle, M.E. (2019). On time delay estimation and sampling error in resting-state fMRI. Neuroimage *194*, 211–227.

Righi, G., Peissig, J.J., and Tarr, M.J. (2012). Recognizing disguised faces. Vis. Cogn. *20*, 143–169.

Ring, H.A., and Serra-Mestres, J. (2002). Neuropsychiatry of the basal ganglia. J. Neurol. Neurosurg. Psychiatry *72*, 12–21.

Rinne, P., Hassan, M., Fernandes, C., Han, E., Hennessy, E., Waldman, A., Sharma, P., Soto, D., Leech, R., Malhotra, P.A., and Bentley, P. (2018). Motor dexterity and strength depend upon integrity of the attention-control system. Proc. Natl. Acad. Sci. USA *115*, E536–E545.

Rosvall, M., and Bergstrom, C.T. (2008). Maps of random walks on complex networks reveal community structure. Proc. Natl. Acad. Sci. U.S.A. *105*, 1118–1123.

Saalmann, Y.B., Pinsk, M.A., Wang, L., Li, X., and Kastner, S. (2012). The pulvinar regulates information transmission between cortical areas based on attention demands. Science *337*, 753–756.

Sadaghiani, S., and D'Esposito, M. (2015). Functional Characterization of the Cingulo-Opercular Network in the Maintenance of Tonic Alertness. Cereb. Cortex *25*, 2763–2773.

Satterthwaite, T.D., Elliott, M.A., Gerraty, R.T., Ruparel, K., Loughead, J., Calkins, M.E., Eickhoff, S.B., Hakonarson, H., Gur, R.C., Gur, R.E., and Wolf, D.H. (2013). An improved framework for confound regression and filtering for control of motion artifact in the preprocessing of resting-state functional connectivity data. Neuroimage *64*, 240–256.

Seitzman, B.A., Gratton, C., Laumann, T.O., Gordon, E.M., Adeyemo, B., Dworetsky, A., Kraus, B.T., Gilmore, A.W., Berg, J.J., Ortega, M., et al. (2019). Trait-like variants in human functional brain networks. Proc. Natl. Acad. Sci. USA *116*, 22851–22861.

Selemon, L.D., and Goldman-Rakic, P.S. (1985). Longitudinal topography and interdigitation of corticostriatal projections in the rhesus monkey. J. Neurosci. *5*, 776–794.

Shipp, S. (2001). Corticopulvinar connections of areas V5, V4, and V3 in the macaque monkey: a dual model of retinal and cortical topographies. J. Comp. Neurol. *439*, 469–490.

Shipp, S. (2004). The brain circuitry of attention. Trends Cogn. Sci. *8*, 223–230.

Siegel, J.S., Snyder, A.Z., Metcalf, N.V., Fucetola, R.P., Hacker, C.D., Shimony, J.S., Shulman, G.L., and Corbetta, M. (2014). The circuitry of abulia: insights from functional connectivity MRI. Neuroimage Clin. *6*, 320–326.

Skogseid, I.M. (2014). Dystonia–new advances in classification, genetics, pathophysiology and treatment. Acta Neurol. Scand. Suppl. *198*, 13–19.

Smith, S.M., Jenkinson, M., Woolrich, M.W., Beckmann, C.F., Behrens, T.E., Johansen-Berg, H., Bannister, P.R., De Luca, M., Drobnjak, I., Flitney, D.E., et al. (2004). Advances in functional and structural MR image analysis and implementation as FSL. Neuroimage *23* (*Suppl 1*), S208–S219.

Starr, P.A., Turner, R.S., Rau, G., Lindsey, N., Heath, S., Volz, M., Ostrem, J.L., and Marks, W.J., Jr. (2006). Microelectrode-guided implantation of deep brain stimulators into the globus pallidus internus for dystonia: techniques, electrode locations, and outcomes. J. Neurosurg. *104*, 488–501.

Tolleson, C., Pallavaram, S., Li, C., Fang, J., Phibbs, F., Konrad, P., Hedera, P., D'Haese, P.F., Dawant, B.M., and Davis, T.L. (2015). The optimal pallidal target in deep brain stimulation for dystonia: a study using a functional atlas based on nonlinear image registration. Stereotact. Funct. Neurosurg. *93*, 17–24.

Van Essen, D.C. (2005). A Population-Average, Landmark- and Surface-based (PALS) atlas of human cerebral cortex. Neuroimage *28*, 635–662.

Van Essen, D.C., Glasser, M.F., Dierker, D.L., Harwell, J., and Coalson, T. (2012). Parcellations and hemispheric asymmetries of human cerebral cortex analyzed on surface-based atlases. Cereb. Cortex *22*, 2241–2262.

van Westen, M., Rietveld, E., Figee, M., and Denys, D. (2015). Clinical Outcome and Mechanisms of Deep Brain Stimulation for Obsessive-Compulsive Disorder. Curr. Behav. Neurosci. Rep. *2*, 41–48.

Vidailhet, M., Vercueil, L., Houeto, J.L., Krystkowiak, P., Benabid, A.L., Cornu, P., Lagrange, C., Tézenas du Montcel, S., Dormont, D., Grand, S., et al.; French Stimulation du Pallidum Interne dans la Dystonie (SPIDY) Study Group (2005). Bilateral deep-brain stimulation of the globus pallidus in primary generalized dystonia. N. Engl. J. Med. *352*, 459–467.

Weller, R.E., Steele, G.E., and Kaas, J.H. (2002). Pulvinar and other subcortical connections of dorsolateral visual cortex in monkeys. J. Comp. Neurol. *450*, 215–240.

Wichmann, T., and Delong, M.R. (2011). Deep-Brain Stimulation for Basal Ganglia Disorders. Basal Ganglia *1*, 65–77.

Wodarg, F., Herzog, J., Reese, R., Falk, D., Pinsker, M.O., Steigerwald, F., Jansen, O., Deuschl, G., Mehdorn, H.M., and Volkmann, J. (2012). Stimulation site within the MRI-defined STN predicts postoperative motor outcome. Mov. Disord. *27*, 874–879.

Worsley, K.J. (1996). The geometry of random images. Chance *9*, 27–40.

Yan, C.G., Cheung, B., Kelly, C., Colcombe, S., Craddock, R.C., Di Martino, A., Li, Q., Zuo, X.N., Castellanos, F.X., and Milham, M.P. (2013). A comprehensive assessment of regional variation in the impact of head micromovements on functional connectomics. Neuroimage *76*, 183–201.

Yeo, B.T., Krienen, F.M., Sepulcre, J., Sabuncu, M.R., Lashkari, D., Hollinshead, M., Roffman, J.L., Smoller, J.W., Zöllei, L., Polimeni, J.R., et al. (2011). The organization of the human cerebral cortex estimated by intrinsic functional connectivity. J. Neurophysiol. *106*, 1125–1165.

Zaaroor, M., Sinai, A., Goldsher, D., Eran, A., Nassar, M., and Schlesinger, I. (2018). Magnetic resonance-guided focused ultrasound thalamotomy for tremor: a report of 30 Parkinson's disease and essential tremor cases. J. Neurosurg. *128*, 202–210.

Zhang, D., Snyder, A.Z., Fox, M.D., Sansbury, M.W., Shimony, J.S., and Raichle, M.E. (2008). Intrinsic functional relations between human cerebral cortex and thalamus. J. Neurophysiol. *100*, 1740–1748.

CellPress

STAR★METHODS

KEY RESOURCES TABLE

REAGENT or RESOURCE	SOURCE	IDENTIFIER
Deposited Data		
Raw and processed MRI data	Gordon et al., 2017b	https://openneuro.org/datasets/ds000224
		Accession # ds000224
Task fMRI activations	Gordon et al., 2017b	https://neurovault.org/collections/2447/
Psychological Image Collection at Stirling 2D face set		http://pics.psych.stir.ac.uk/
CNBC Tarrlab "Face Place" repository	Righi et al., 2012	https://wiki.cnbc.cmu.edu/Face_Place
Park Aging Mind Laboratory Face Database		agingmind.utdallas.edu/facedb
Libor Spacek's Facial Imaging Database		cmp.felk.cvut.cz/~spacelib/faces/
English Lexicon Project	Balota et al., 2007	https://elexicon.wustl.edu/
Software and Algorithms		
MATLAB	Mathworks	RRID:SCR_001622 https://www.mathworks.com/
Connectome Workbench	Marcus et al., 2011	RRID:SCR_008750 http://www.humanconnectome.org/software/connectome-workbench.html
Freesurfer	Dale et al., 1999	RRID:SCR_001847 https://surfer.nmr.mgh.harvard.edu/
FSL	Smith et al., 2004	RRID:SCR_002823 https://fsl.fmrib.ox.ac.uk/fsl/fslwiki
4dfp tools		ftp://imaging.wustl.edu/pub/raichlab/4dfp_tools/
Freesurfer to fs_LR pipeline	Van Essen et al., 2012	http://brainvis.wustl.edu/index.html/
Parcellation code	Gordon et al., 2016	https://sites.wustl.edu/petersenschlaggarlab
Infomap	Rosvall and Bergstrom, 2008	https://www.mapequation.org/

LEAD CONTACT AND MATERIALS AVAILABILITY

Further information and requests for resources should be directed to and will be fulfilled by the Lead Contact, Deanna Greene (dgreene@wustl.edu)

EXPERIMENTAL MODEL AND SUBJECT DETAILS

Data from ten young adults (24-34 years old; 5 females; all right handed) from the publicly available Midnight Scan Club (MSC) dataset were used in the present study (https://openneuro.org/datasets/ds000224). Details about the dataset and processing have been previously described (Gordon et al., 2017b). Here, we describe information about the data and processing that is relevant to the current project, and the specific analyses employed.

Participants and Study Design

The MSC dataset includes structural and functional MRI data, as well as behavioral measures from 10 individuals (5 females, ages 24-34). fMRI data were collected over 10 sessions, each occurring on a separate day, beginning at midnight. Daily sessions were conducted in close succession, with all sessions completed within 7 weeks for all participants. All participants provided written informed consent. Procedures were approved by the Washington University Institutional Review Board and School of Medicine Human Studies Committee. During each scanning session, participants completed a 30 min resting-state run followed by fMRI scans during four other tasks: a motor task, a semantic task, a coherence task, and an incidental encoding memory task. MRI acquisition parameters and tasks are described below.

METHOD DETAILS

MRI image acquisition

Participants underwent 12 imaging sessions on a Siemens TRIO 3T MRI scanner, beginning at midnight, over the course of 3-6 weeks each. The first two sessions consisted of structural MRI scans and the following ten sessions consisted of functional MRI (fMRI) scans. Structural images included four T1-weighted scans (TE = 3.74ms, TR = 2400ms, TI = 1000ms, flip angle = 8°, 0.8mm isotropic voxels, 224 sagittal slices), four T2-weighted images (TE = 479ms, TR = 3200ms, 0.8mm isotropic voxels, 224 sagittal, 224), four MRA and eight MRV scans (not used in the present study; see Gordon et al., 2017b for details). Functional images included 300min total of eyes-open resting-state fMRI BOLD data (30min per session) and 350min total of task fMRI BOLD data (see below) using a gradient-echo EPI BOLD sequence (TE = 27ms, TR = 2.2 s, flip angle = 90°, 4mm isotropic voxels, 36 axial slices). Gradient echo field map images (one per session) were acquired with the same parameters.

One participant (MSC06) underwent an additional 12 imaging sessions on a Siemens Prisma 3T MRI scanner, consisting of fMRI scans with higher resolution (gradient-echo EPI BOLD sequence: multiband factor 4, TE = 33ms, TR = 1.1 s, flip angle = 84°, 2.6mm isotropic voxels, 56 axial slices).

QUANTIFICATION AND STATISTICAL ANALYSIS

MRI Data Processing and Surface Registration

MRI data were preprocessed and sampled to the cortical surface as previously described in detail (Marek et al., 2018). The processing code is code is publicly available at https://github.com/MidnightScanClub. Here, we briefly describe the steps.

Structural MRI

Cortical surfaces were generated using procedures as in Laumann et al. (2015). Briefly, using FreeSurfer v5.3, each subject's averaged T1-weighted image was run through the recon-all processing pipeline to generate the anatomical surface (Dale et al., 1999; Fischl et al., 1999). This surface was manually edited using Freeview to maximize accuracy, and registered into fs_LR_32k surface space using a flexible Multi-modal Surface Matching algorithm (Glasser et al., 2016; Van Essen et al., 2012). The subject-specific surfaces in native space were transformed into Talairach volumetric space by applying an average T1-to-Talairach transform.

Functional MRI preprocessing

All functional data were preprocessed in volume space to reduce artifact and maximize cross-session registration, including (i) slice timing correction, (ii) intensity normalization to a whole brain mode value (across voxels and TRs) of 1000 for each run, and (iii) within-run correction for head motion. Then, the functional data were registered to Talairach atlas space using the average T2-weighted image and the average T1-weighted image. Distortion correction was applied using a mean field map for each subject and applying that field map to each fMRI session, as previously described (Gordon et al., 2017b). Registration, atlas transformation, distortion correction, and resampling to 3mm isotropic atlas space were combined into a single interpolation using FSL's applywarp tool (Smith et al., 2004). To account for anatomical differences between subjects, we non-linearly warped each subject's atlas-aligned T1 to MNI space using FSL's FNIRT. Volumetric time series subsequently were registered to each subject's registered T1. All between subjects analyses and group average analyses were carried out on these atlas-transformed volumetric time series.

Functional connectivity preprocessing

Additional preprocessing steps were applied to the resting-state fMRI data to reduce spurious variance unlikely to reflect neuronal activity. First, a motion censoring procedure as described in Power et al. (2014) was implemented, which in combination with our other processing steps has been shown to best account for motion artifact (Ciric et al., 2017). Temporal masks were created to flag motion-contaminated volumes based on framewise displacement (FD) and the temporal derivative of the root mean squared variance over voxels (DVARS). Frames with FD > 0.2mm or DVARS > 5.36 were flagged. Two subjects (MSC03, MSC10) required additional correction for artifactual high-frequency motion in the phase encoding direction (anterior-posterior) as previously described (Gordon et al., 2017b; Gratton et al., 2018). Application of the temporal masks resulted in retention of 5704 ± 1548 volumes per subject (range 2691-7530) (for more details, see Gordon et al., 2017b). Thus, even the subject with the most motion-contaminated data retained nearly 100 min. Then, the data underwent additional processing steps, including (i) demeaning and detrending, (ii) interpolation across censored volumes using least-squares spectral estimation of the values at the censored time points, (iii) temporal band-pass filtering (0.005 Hz < f < 0.01 Hz), and (iv) multiple regression of nuisance variables, including the global signal, principle components of ventricular and white matter signals (see below "Component-based nuisance regression"), and motion estimates derived by Volterra expansion (Friston et al., 1996), applied in a single step to the filtered, interpolated BOLD time series. Finally, censored volumes were removed from the data for all subsequent analyses.

For the additional 2.6mm resolution data collected from MSC06, the data were processed the same as the 4mm resolution data, with the following exceptions: (1) FD measurements were corrected for artifactual high-frequency motion in the phase encoding direction, (2) the FD threshold for motion censoring was 0.1mm, and (3) the DVARS threshold for motion censoring was 6.

CellPress

The cortical data were then registered to the surface (see above, *Structural MRI*). The cortical surface data and volumetric subcortical and cerebellar data were combined into CIFTI data format using Connectome Workbench (Marcus et al., 2011). Voxels in the cerebellum and subcortex (including thalamus, caudate, putamen, pallidum, nucleus accumbens, amygdala, and hippocampus) were derived from the FreeSurfer segmentation of each subject's native average T1 image, transformed into Talairach atlas space. Finally, the cortical surface functional data were smoothed (2D geodesic, Gaussian kernel, σ = 2.55mm). Due to the relatively small size of the basal ganglia and thalamus, we did not perform spatial smoothing within the volume and we up-sampled the fully processed data to 2mm isotropic voxels. To mitigate effects of signal contamination from nearby cortical areas (e.g., insula signal adjacent to the putamen), we regressed the time course of BOLD activity from any cortical vertices within 20mm of a subcortical voxel, similar to strategies taken in previous work on subcortical functional connectivity (Choi et al., 2012; Greene et al., 2014).

Component-based nuisance regression

The filtered BOLD time series underwent a component-based nuisance regression approach as in Marek et al. (2018) and Raut et al. (2019), incorporating elements of previously published methods (Behzadi et al., 2007). Nuisance regressors were extracted from individualized white matter and ventricle masks, first segmented by FreeSurfer (Fischl, 2012), then spatially resampled in register with the fMRI data. Since voxels surrounding the edge of the brain are particularly susceptible to motion artifacts and CSF pulsations (Satterthwaite et al., 2013; Yan et al., 2013), a third nuisance mask was created for the extra-axial compartment (edge voxels; Patriat et al., 2015) by thresholding the temporal standard deviation image (SDt > 2.5%) (Behzadi et al., 2007), excluding a dilated whole brain mask. Voxel-wise nuisance time series were dimensionality reduced as in CompCor (Behzadi et al., 2007), except that the number of retained regressors, rather than being a fixed quantity, was determined, for each noise compartment, by orthogonalization of the covariance matrix and retaining components ordered by decreasing eigenvalue up to a condition number of 30 $((\lambda_{max}/\lambda_{min}) > 30)$. The retained components across all compartments formed the columns of a design matrix, X, along with the global signal, its first derivative, and the six time series derived by retrospective motion correction. The columns of X are likely to exhibit substantial co-linearity. Therefore, to prevent numerical instability owing to rank-deficiency during nuisance regression, a second-level SVD was applied to XX^T to impose an upper limit of 250 on the condition number. This final set of regressors was applied in a single step to the filtered, interpolated BOLD time series.

Analysis Overview
Cortico-subcortical FC

To capture cortico-subcortical resting state functional connectivity (RSFC), we measured RSFC between subcortical voxels and cortical functional networks. First, we identified each subject's individual cortical functional network organization using the graph-theory-based Infomap algorithm for community detection (Rosvall and Bergstrom, 2008), following Power et al. (2011). Derivation of the Infomap communities (representing networks) for each subject has been previously described in Gordon et al. (2017b) and Marek et al. (2018). Briefly, Pearson r correlations were computed between the BOLD time series (concatenated across sessions) among all cortical vertices, generating a 59,412 vertex x 59,412 vertex correlation matrix. The matrix was thresholded across a range of densities from 0.1% to 5%, and community assignments were generated from the Infomap algorithm for each threshold. To assign putative network identities to each subject's communities, a matching procedure to networks identified for an independent group of 120 subjects was used (see Gordon et al., 2017b; Marek et al., 2018 for details). Figure 8A shows these cortical functional network assignments for each individual subject and for the group average.

For the purposes of our subcortical-cortical analyses, we selected nine cortical functional networks (the same 9 for all subjects) that have been previously well-characterized in the cortex by multiple investigators using varying methods (e.g., Damoiseaux et al., 2006; Gordon et al., 2016; Power et al., 2011; Yeo et al., 2011) and have been examined with respect to RSFC with the subcortex (Greene et al., 2014): somatomotor hand, somatomotor face, visual, frontoparietal, cingulo-opercular, dorsal attention, ventral attention, salience, and default-mode. These cortical networks are shown for each subject in Figure 8A. Then, we computed the average time series across vertices for each of these nine cortical networks in each hemisphere separately, and correlated them with the time series from each subcortical voxel (voxels within each subject's thalamus, caudate, putamen, pallidum, and nucleus accumbens; Figure 8B) in the ipsilateral hemisphere (consistent with anatomical connections). Note that our results do not appreciably change when the analyses are conducted using correlations from both hemispheres (83% of subcortical voxels have identical "winning" network assignments). Given the close anatomical proximity of several subcortical structures to certain regions of cortex, we regressed the cortical signal within 20mm of the subcortex from each subcortical voxel time series in order to mitigate potential artifactual inflations in correlations due to signal bleed, similar to previous subcortical-cortical RSFC studies (Choi et al., 2012; Greene et al., 2014). The resulting subcortical voxel-to-cortical network correlation matrices (one per subject) were used for subsequent analyses.

The same procedures were applied to the whole group of subjects in order to compute the group averaged subcortical voxel-to-cortical network correlation matrix. The nine cortical functional networks were selected from the group average Infomap communities as reported in Marek et al. (2018).

We repeated these procedures after partialing out the time series of activity of each cortical network from every other network (as in Greene et al., 2014) before quantifying RSFC between each subcortical voxel and cortical network. Voxel-wise results were highly similar (r = 0.75) between approaches using full correlations and partial correlations. We also repeated these procedures using

the 15-networks Infomap solution (excluding unassigned vertices and medial temporal lobe vertices due to proximity to the subcortex; Figure S8B left) as well as using a 7-network Infomap solution (Figure S8A left).

In addition, we compared the correlation results against a null model using randomly rotated cortical networks, similar to (Gordon et al., 2017a; Gordon et al., 2016). First, for each subject we randomly rotated that subject's cortical networks around the spherical expansion of the cortical surface to produce cortical objects that had the same size, shape, and spatial distribution as real networks, but in random locations. Next, for every subcortical voxel, we calculated the average correlation to each rotated cortical network, excluding portions of the rotated networks that fell on the medial wall or in susceptibility artifact regions. This rotation and calculation of correlations was repeated 1000 times, generating a null distribution of correlations. Finally, for each network-subcortical voxel connection, we calculated the percent of iterations for which the correlation to the real network was stronger than the correlation to that iteration's rotated version of that network. This value represents the likelihood that a voxel's correlation to a cortical network is stronger than would be expected if the cortical network location was randomized. We compared this "percent stronger than null" map to the standard functional connectivity correlation maps for each network for each subject.

Reliability of cortico-subcortical FC

Using an iterative split-half reliability analysis similar to (Gordon et al., 2017b; Laumann et al., 2015), we computed each individual subject's reliability of cortico-subcortical RSFC. For each subject, the ten scan sessions were randomly divided into two subsets of five sessions each. Half of the data (motion censored) was randomly selected from one of the subsets to serve as the comparison data, and a varying amount of data (5 to 100 minutes in 5 minute increments) was randomly selected from the other subset to serve as the test data. Reliability was estimated by computing the average correlation between the subcortical voxel-to-cortical network matrices for the comparison and test data. This procedure was iterated 1000 times using different subsets of random data (i.e., random halves of the data) in each iteration.

As some regions within the subcortex may have better reliability than others, we conducted a voxelwise split-half reliability analysis. For each subject, the ten scan sessions were randomized, concatenated, split into two halves, and the subcortical voxel-to-cortical network correlation matrices were computed for each half. Reliability for each voxel was estimated by computing the correlation between the halves. We also tested the relationship between reliability and tSNR by correlating these two measures across voxels for each subject. In order to mitigate the effects of voxels with relatively poor reliability, subsequent analyses excluded those voxels with reliability < 0.5 for each subject.

Task activations

Task fMRI data were processed as previously described (Gordon et al., 2017b; Gratton et al., 2018). Briefly, the cognitive/perceptual tasks consisted of a pair of mixed block/event-related design tasks that began with a task cue followed by a block of jittered trials in each task, modeled after Dubis et al. (2016). The "language" task trials consisted of single words and participants were asked to determine whether the words were nouns or verbs. The "perceptual" task consisted of Glass dot patterns (Glass, 1969) at either 50% or 0% coherence. Participants were asked to determine whether or not the dots were arranged concentrically. The motor task, modeled after the HCP motor task (Barch et al., 2013), consisted of blocks of movements of either left or right hand, left or right foot, or the tongue.

After standard fMRI preprocessing, task fMRI data were entered in a General Linear Model (GLM) separately for each session from each individual using in-house IDL software (FIDL) (Miezin et al., 2000). The mixed design tasks were modeled jointly in a single GLM with separate event regressors for onset and offset cues from each task, trials in each task (nouns and verbs for the cognitive task, 0% and 50% for the perceptual task), and a sustained block regressor for the task period. Event regressors were modeled using a finite impulse response approach consisting of delta functions at each of 8 time points, allowing for the more complete modeling of different HRF shapes (Ollinger et al., 2001). The motor task was modeled with separate block regressors for each motor condition.

Deactivations associated with the default mode network were identified using a contrast of the third and fourth time points from all conditions in the mixed design tasks (against an implicit, unmodeled, baseline). Activations associated with the somatomotor hand network were identified using a contrast between left and right hand movement blocks with left and right foot movement blocks.

Similarity analysis

Similarity analyses were carried out similar to Gratton et al. (2018) and Marek et al. (2018). For each subject, the ten scan sessions were randomized, split into two halves, and concatenated. The subcortical voxel-to-cortical network correlation matrices were computed for each half and vectorized. Then the similarity (Pearson z(r)) between the two halves of data was calculated both within split halves of an individual's data and between split halves of every other individual. This analysis resulted in a similarity matrix, in which off-diagonal elements represent variance shared across individuals (i.e., group effect), and on-diagonal elements represent variance shared across scanning sessions within an individual. Variance unique to individuals versus the group was quantified by normalizing (dividing) variance shared across individuals (group effect; off-diagonal elements) by subject similarity (on-diagonal elements). The production of similarity matrices and quantification of group versus individual level effects were computed separately for the basal ganglia and thalamus.

We also examined between-subject variability in the subcortex as we have previously done in the cortex (Laumann et al., 2015) and cerebellum (Marek et al., 2018). We calculated the standard deviation of correlations between each subcortical voxel and every cortical network across subjects. We then assigned each subcortical voxel to a single network (standard winner-take-all approach)

CellPress

in order to compare the standard deviation of higher-order network subcortical voxels (frontoparietal, dorsal attention, ventral attention, salience, cingulo-opercular, default-mode) to that of processing network subcortical voxels (visual, somatomotor hand, somatomotor face) using a t test.

Network specificity versus integration

To determine which subcortical voxels were "network-specific" versus "integrative" we implemented a modified winner-take-all analysis. For each subject, a "winning" network was assigned to each subcortical voxel based on the strength of the correlation between that voxel and each cortical network. The network with the strongest correlation was deemed the winner. Then, we categorized a voxel as network-specific if its correlations with all other networks were less than 2/3 (66.7%) of its correlation with the winning network, in line with Marek et al. (2018). If this criterion was not met, the voxel was categorized as integrative, and those networks within 2/3 of the winning network were also considered winners. This procedure yielded multiple networks (minimum two networks; maximum four networks – note that there was no instance with more than four networks) within an integrative voxel, whereas a network-specific voxel, by definition, was occupied by one network. Given the somewhat arbitrary nature of the 66.7% threshold, we also tested 50% and 75%, which resulted in highly similar distributions of network-specific versus integrative functional zones (see Figure S6A).

In addition, we tested an alternative approach for determining network specificity versus integration based on effect size (Cohen's d). For every subcortical voxel, we computed t tests comparing its correlations with the winning network (all cortical vertices within that network) to its correlations with every other network (all cortical vertices within a subsequent network). Thus, we were able to compute the effect size of each comparison. Voxels were determined to be network-specific versus integrative based on whether the observed effect size between the winning network and another network was greater than or less than a benchmarked effect size. In Figure S6B, we show the resulting zones of integration for small ($d = 0.2$), medium ($d = 0.5$), and large ($d = 0.8$) effect sizes. This approach yielded similar zones of integration to the original approach described in the previous paragraph. Thus, our main results are reported using the original approach at a threshold of 66.7%.

Pictorially in Figure 3, network-specific voxels were colored by their affiliated network, whereas integrative voxels were colored by each network represented in that voxel (striped pattern). For integrative voxels, the base color was determined by the network assigned to that voxel in separate, previously described group-averaged data (WashU 120) using a standard winner-take-all method (basal ganglia winner-take-all parcellations previously reported in Greene et al., 2014). Thus, if a network represented in an integrative voxel was shared with the network assigned to that voxel in the WashU 120, the voxel's base color was assigned to that network, and the other networks were shown as thin stripes. If none of the networks were shared with the WashU 120, the base color was assigned to the network with the strongest correlation.

One concern arising from delineating integration zones within the subcortex is the spatial proximity of networks given the relatively smaller size of subcortical structures. To test for the presence of integration rather than solely proximity to multiple networks, we performed a community density analysis across the subcortex. Using the winning network assignment for each subcortical voxel from the winner-take-all analysis, community density was determined by counting the number of networks within a spotlight of 3mm. If integration was largely due to high community density, the majority of high community density voxels would be expected to be integrative. To test this prediction, for each subject we extracted all voxels with a community density > 1, which indicates the presence of at least one neighboring voxel with a different network assignment, and calculated the percent of those voxels that were integrative.

Quantification of network specificity and integration across functional networks

To examine how network specificity and integration were distributed across functional networks, we quantified the number of network-specific and integrative voxels for each network. We generated a network-by-network matrix representing the number of voxels, summed across subjects, that were integrative for all pairs of networks (e.g., number of integrative voxels containing frontoparietal and salience networks). We normalized these summed values by the total number of integrative voxels, resulting in a percentage of integrative voxels for each network combination. We calculated these percentages separately for each structure. We determined the degree to which functional networks cluster with respect to patterns of integration (i.e., extent to which certain networks preferentially integrated with each other). To this end, we performed a hierarchical clustering analysis using MATLAB's *linkage, pdist,* and *dendrogram* functions, with default setting for determining the optimal cluster solution. We validated the clusters produced by the hierarchical clustering analysis by submitting the network-by-network matrix to a graph theoretic clustering analysis (modularity) (Newman, 2006), replicating a three cluster solution.

Defining functional zones in the subcortex

Having determined network-specific and integrative subcortical voxels for each subject, we aimed to identify zones of network specificity and integration that were common across the group versus variable across individuals. First, a voxel was considered network-specific if that voxel was network-specific in > 5 subjects. A voxel was considered integrative if that voxel was integrative in > 5 subjects. If a voxel met neither criteria, it was not assigned to a zone. For the assigned voxels, we next determined whether they exhibited RSFC that was common across the group (Group) or varied across individuals (Individual). For network-specific voxels, they were considered Group if > 5 subjects shared the same network assignment; otherwise, they were considered Individual. For integrative voxels, they were considered Group if at least two of the networks assigned to that voxel were present in > 5 subjects; otherwise, they were considered Individual. Thus, we defined four voxel types: Group Network-specific, Group Integrative, Individual Network-specific, and Individual Integrative. To delineate functional zones, we applied a cluster threshold of 20 voxels and removed

extraneous voxels that did not share more than one face with other voxels in that cluster, i.e., ensuring a Euler characteristic of two (Worsley, 1996).

To determine the stability of these functional zones, we performed a jack-knifing procedure. The steps just described for defining the four zones were repeated ten times, leaving out a unique subject with each iteration. We then calculated the percent of iterations that each voxel was assigned to each of the four zone types. Thus, we estimated confidence in functional zone assignment (Figure 6A).

Functional zone examples

To display examples of each of the four types of functional zones, we selected an example voxel within each type (Figure 6A). Figure 6B displays the correlations from these voxels to all cortical vertices on the cortical surface with subject-specific Infomap network borders for two representative subjects, as well as the strength of the correlations to each cortical network.

DATA AND CODE AVAILABILITY

The ''Midnight Scan Club'' data (raw and processed) used in the present study are available in the OpenfMRI data repository at https://openneuro.org/datasets/ds000224. The accession number for the Midnight Scan Club data reporte din this paper is ds000224. Processing and analysis code is available at https://github.com/MidnightScanClub/MSCcodebase.